International Journal of Multiphase Flow 34 (2008) 1067–1087

Contents lists available at ScienceDirect

International Journal of Multiphase Flow

journal homepage: www.elsevier.com/locate/ijmulflow

A study on the numerical stability of the two-fluid model near ill-posedness

Jun Liao [1], Renwei Mei, James F. Klausner *

Department of Mechanical & Aerospace Engineering, University of Florida, P.O. Box 116300, Gainesville, FL 32611-6300, USA

ARTICLE INFO

Article history:
Received 12 September 2007
Received in revised form 15 January 2008
Accepted 2 February 2008
Available online 17 July 2008

Keywords:
Two-fluid model
Instability
Ill-posedness

ABSTRACT

The two-fluid model is widely used in studying gas–liquid flow inside pipelines because it can qualitatively predict the flow field at low computational cost. However, the two-fluid model becomes ill-posed when the slip velocity exceeds a critical value, and computations can be quite unstable before the flow reaches the ill-posed condition. In this work, computational stability of various convection schemes together with the Euler implicit method for the time derivatives in conjunction with the two-fluid model is analyzed. A pressure correction algorithm for the two-fluid model is carefully implemented to minimize its effect on numerical stability. von Neumann stability analysis shows that the central difference scheme is more accurate and more stable than the 1st-order upwind, 2nd-order upwind, and QUICK schemes. The 2nd-order upwind scheme is much more susceptible to instability than the 1st-order upwind scheme and is inaccurate for short waves. Excellent agreement is obtained between the predicted and computed growth rates of harmonic disturbances. The instability associated with the two-fluid model discretized system of equations is related to but quantitatively different from the instability associated with ill-posedness of the two-fluid model. When the computation becomes unstable due to the ill-posedness, the machine roundoff errors from a selected range of short wavelengths, which scale with the grid size, are amplified rapidly to render the computation of any targeted long wavelength variation useless. For the viscous two-fluid model with wall friction and interfacial drag, a small-amplitude long wavelength disturbance grows due to viscous Kelvin–Helmholtz instability without triggering the grid scale short waves when the system remains well posed. Under such a condition, central difference is found to be the most accurate discretization scheme among those investigated.

1. Introduction

Gas–liquid flow inside a horizontal pipeline is prevalent in the handling and transportation of fluids. A reliable flow model is essential to the prediction of the flow field inside the pipeline. To fully simulate the system, Navier–Stokes equations in three-dimensions are required for each phase. However, it is very expensive to simulate flows in long pipelines with contemporary computer capabilities. To reduce the computational cost and obtain basic flow properties, such as gas volume fraction, liquid and gas velocity, and pressure, a one-dimensional two-fluid model is often used to obtain a realistic prediction for the gas–liquid flow inside a pipeline.

The separated flow model, one common type of two-fluid model, consists of two sets of conservation equations for mass, momentum and energy for the gas phase and the liquid phase. It was proposed by Wallis (1969), and further refined by Ishii (1975). Although it has demonstrated success in simulating two-phase flow in a pipeline, the separated flow model, hereafter referred to as the "standard" two-fluid model, suffers from an ill-posedness problem. When the relative velocity between the liquid and gas exceeds a critical value, the governing equations do not possess real characteristics (Gidaspow, 1974; Ramshaw and Trapp, 1978; Jones and Prosperetti, 1985; Song and Ishii, 2000). This ill-posedness suggests that the results of the standard two-fluid model do not reflect the real flow physics inside the pipe for those conditions. The standard two-fluid model only gives meaningful results when the relative velocity between the gas phase and liquid phase is less than a critical value, which depends on pipe diameter, gravity, and liquid level, among other flow properties. However, this critical value coincides with the inviscid Kelvin–Helmholtz (IKH) stability condition for stratified flow (Issa and Kempf, 2003). Because the occurrence of the instability characterizes a flow regime transition from stratified flow to slug flow or annular flow (Barnea and Taitel, 1994), ill-posedness of the standard two-fluid model is interpreted as triggering the flow regime transition (Barnea and Taitel, 1994; Brauner and Maron, 1992).

The computational methods for solving the standard two-fluid model have been investigated by many researchers. In this study, it is further assumed that both liquid and gas phases are incompressible because most of stratified flows are at relatively low

* Corresponding author. Tel.: +1 352 392 3506; fax: +1 352 392 1071.
E-mail address: klaus@ufl.edu (J.F. Klausner).
[1] Present address: Westinghouse Electric Company, 4350 Northern Pike, Monroeville, PA 15146, USA.

0301-9322/$ - see front matter © 2008 Elsevier Ltd. All rights reserved.
doi:10.1016/j.ijmultiphaseflow.2008.02.010

speed compared with the speed of sound. To solve the incompressible standard two-fluid model equations, Newton iteration is commonly used (Liles and Reed, 1978; Mahaffy, 1982). However, the complexity associated with the Jacobian compromises the efficiency of this approach. Another approach is to simplify the governing system to only two equations for the liquid phase volume fraction and liquid velocity and neglect the transient terms in the gas mass and momentum equations (Barnea and Taitel, 1994; Chan and Banerjee, 1981). The pressure correction scheme (Patankar, 1980) has recently been implemented by various researchers (Issa and Woodburn, 1998; Issa and Kempf, 2003; Ansari and Shokri, 2007) for solving the standard two-fluid model.

When the standard two-fluid model becomes ill-posed due to high slip velocity, the analytical solution for any specified initial disturbance grows indefinitely and does not carry any physical meaning. When a numerical scheme employed to solve the standard two-fluid model becomes unstable, the magnitude of the numerical error increases at a faster rate than the growth rate of the physical solution and similarly the solution does not carry any meaning. However, numerical instability may not be quantitatively the same as the instability caused by the ill-posedness, and the numerical instability may occur earlier than the ill-posedness condition, depending on how the system of equations is discretized. Thus, a thorough investigation on the numerical instability of the standard two-fluid model is desirable.

Lyczkowski et al. (1978) used von Neumann stability analysis to study a compressible two-fluid model in conjunction with their numerical scheme and found that numerical instability and ill-posedness may not be identical. However, their two-fluid model lacked the gravitational term and the study focused on one discretization scheme and is thus incomplete. Stewart (1979), Ohkawa and Tomiyama (1995) and Shieh (1994) attempted to analyze the numerical stability of a two-fluid model with a simplified model equation as an alternative. Ohkawa and Tomiyama (1995) demonstrated that a higher order upwind scheme yields a more unstable numerical solution than the 1st-order upwind scheme based on solutions of the simplified model.

Issa and Kempf (2003) used the donor-cell scheme for the convection term and the pressure-correction method (Patankar, 1980) for coupling the velocity to the pressure in solving the inviscid and viscous two-fluid models. They also found that when the system is ill-posed, which coincides with the inviscid Kelvin–Helmholtz (IKH) instability, the refinement of the grids leads to a higher growth rate of the solution. Since viscous Kelvin–Helmholtz (VKH) instability is triggered at a lower slip velocity than that for the IKH instability (Lin and Hanratty, 1986, 1987), the system can still be well-posed while a small disturbance grows in time for a range of slip velocity. Within this range, Issa and Kempf (2003) simulated the transition from stratified to slug flow using a viscous two-fluid model employing the donor-cell difference scheme.

Donor-cell is a first-order upwind (FOU) scheme which is known to be 1st-order accurate with large numerical dissipation. Certain questions naturally come to the forefront:

- Is the FOU a good scheme for discretizing the convection term when solving the standard two-fluid model system using the pressure-correction method?
- Is the FOU scheme superior comparing with other well known methods such as 2nd-order upwind (SOU), central difference (CD), and quadratic upstream interpolation for convection kinematics (QUICK) schemes?
- Even more importantly, does the 1st-order upwind scheme ensure that the condition for the numerical instability lie as close as possible to the ill-posedness condition so that the transition to slug flow is predicted at the correct slip velocity?

Hwang (2003) presented a detailed mathematical study on the accuracy of numerical schemes for hyperbolic as well as non-hyperbolic model systems. He showed that segregated treatment using the upwind scheme on each equation leads to poor stability. His study also suggested that an accurate numerical solution for a non-hyperbolic system is possible for a limited time, despite the ill-posedness or lack of hyperbolicity of the physical problem. Prosperetti (2007) argued that the loss of hyperbolicity in the standard two-fluid model prevents physically relevant solutions from being obtained; furthermore the numerical solution will be unstable for a disturbance of any wavelength since the machine error induced short waves grow rapidly and eventually dominate the solution.

In order to appreciate Prosperetti's insight and understand how to interpret Hwang's (2003) numerical solution of a non-hyperbolic system before it is dominated by short wave error, it is instructive to carefully examine how the short waves originate and grow. The central questions are:

- For a given numerical algorithm and grid density for the two-fluid model, what wavelength will be naturally selected to grow most rapidly?
- What is the growth rate of the selected short waves?
- How does the non-linearity in the governing equations affect the selected wavelength and the growth rate?
- If the computation survives the rapid growth of the short waves for an ill-posed non-linear problem, can the subsequent numerical solution be trusted?
- How does the interfacial drag between two fluids affect the computational stability when various difference schemes are used?

In this study, an implicit pressure correction scheme is implemented to discretize the two-fluid model equations. Care has been taken so that mass and momentum conservation across each computational cell are strictly enforced. The von Neumann stability analysis is employed to study the stability of the discretized standard inviscid two-fluid model with different interpolation schemes for the convection term. Examination of the wave amplification factors using the FOU, SOU, QUICK, and CD schemes shows that the CD scheme is more accurate and more stable, a result which is not intuitively obvious. The CD scheme gives the critical slip velocity that is very close to the IKH stability criterion—an essential requirement for accurate computation of stratified flow. Excellent agreement for the growth of the wave amplitude is obtained between the von Neumann stability analysis and the actual computation under various conditions for the discretization schemes investigated. For an ill-posed system or when the computation becomes unstable, the growth of a specified primary long wavelength disturbance as well as the growth of the machine roundoff error on a selected group of wavelengths is discussed.

For the standard viscous two-fluid model, the von Neumann stability analysis is used to examine the numerical stability for flow conditions after the VKH instability is triggered. The performance of different discretization schemes used with the standard viscous two-fluid model is compared. The relation between the numerical instability and the VKH instability of the viscous flow two-fluid model is clarified. It is demonstrated that the central difference scheme is most accurate and reliable for the standard viscous two-fluid model among the four discretization schemes investigated.

2. Governing equations

The basis for the standard two-fluid model is a set of one-dimensional conservation equations for the balance of mass, momentum and energy for each phase. The one-dimensional con-

servation equations are obtained by integrating the flow properties over the cross-sectional area of the flow. The schematic depiction of two-phase flow in a horizontal pipe is shown in Fig. 1.

Because the ill-posedness originates from the modeling of the mass and momentum conservations, it is only necessary to consider the continuity and momentum equations in the standard two-fluid model. For simplicity, no mass transfer between phases is implemented. Surface tension is also neglected since it only acts on small scales, while the waves determining the flow structure in a pipe flow are usually of long wavelength. Hence, the governing equations for the standard two-fluid model in a pipeline with constant flow area are as follows:

$$\frac{\partial}{\partial t}(\alpha_l)+\frac{\partial}{\partial x}(u_l\alpha_l)=0, \tag{1}$$

$$\frac{\partial}{\partial t}(\alpha_g)+\frac{\partial}{\partial x}(u_g\alpha_g)=0, \tag{2}$$

$$\frac{\partial}{\partial t}(u_l\alpha_l)+\frac{\partial}{\partial x}(u_l^2\alpha_l)=-\frac{\alpha_l}{\rho_l}\frac{\partial p_i}{\partial x}-g\cos\beta H_l\frac{\partial\alpha_l}{\partial x}-\alpha_l g\sin\beta-\frac{\tau_l S_l}{A\rho_l}+\frac{\tau_i S_i}{A\rho_l}, \tag{3}$$

$$\frac{\partial}{\partial t}(u_g\alpha_g)+\frac{\partial}{\partial x}(u_g^2\alpha_g)=-\frac{\alpha_g}{\rho_g}\frac{\partial p_i}{\partial x}-g\cos\beta H_g\frac{\partial\alpha_l}{\partial x}-\alpha_g g\sin\beta-\frac{\tau_g S_g}{A\rho_g}-\frac{\tau_i S_i}{A\rho_g}, \tag{4}$$

where t and x are the respective time and axial coordinates, α is the volume fraction, u is the velocity, p is the pressure, ρ is the density, g is the gravitational acceleration, β is the pipe inclination angle, τ is the shear stress, S is the perimeter over which τ acts, A is the pipe cross sectional area; the subscripts l and g denote the liquid and gas, respectively, and the subscript i denotes the interface. H_l and H_g are the hydraulic depth, defined as

$$H_l=\frac{\alpha_l}{\partial\alpha_l/\partial h_l}=\frac{\alpha_l}{\alpha_l'}=D\frac{(\varphi-0.5\sin 2\varphi)}{4\sin\varphi}, \tag{5}$$

and

$$H_g=\frac{\alpha_g}{\partial\alpha_g/\partial h_g}=\frac{\alpha_g}{\alpha_g'}=D\frac{\pi-\varphi+0.5\sin 2\varphi}{4\sin\varphi}, \tag{6}$$

where h_l is the liquid layer depth, h_g is the gas layer depth, D is the pipe diameter, and φ is the angle between the interface and the vertical centerline as shown in Fig. 1. It is also noted that

$$\alpha_l+\alpha_g=1. \tag{7}$$

For the standard inviscid two-fluid model, the shear stress terms are zero. Thus the governing equations are Eqs. (1)–(7) without the last two terms in Eqs. (3) and (4).

For the standard viscous two-fluid model, shear stresses τ_l, τ_g and τ_i must be specified to achieve closure. There are many suggested shear stress correlations for the standard two-fluid model. The widely accepted shear stress correlations by Taitel and Dukler (1976) are used in this study:

$$\tau_l=f_l\frac{\rho_l u_l^2}{2},\quad \tau_g=f_g\frac{\rho_g u_g^2}{2},\quad \tau_i=f_i\frac{\rho_g(u_g-u_l)|u_g-u_l|}{2}. \tag{8}$$

Liquid and gas friction factors f are given by

$$f_l=C_l\left(\frac{u_l D_l}{\nu_l}\right)^{-n},\quad f_g=C_g\left(\frac{u_g D_g}{\nu_g}\right)^{-m}, \tag{9}$$

in which hydraulic diameters D_l and D_g are defined as

$$D_l=\frac{4A_l}{S_l},\quad D_g=\frac{4A_g}{S_g+S_i}. \tag{10}$$

The coefficients C_g and C_l are equal to 0.046 for turbulent flow and 16 for laminar flow, while n and m take the values of 0.2 for turbulent flow and 1.0 for laminar flow. The interfacial friction factor is assumed to be $f_i = f_g$ or $f_i = 0.014$ when $f_g < 0.014$.

3. Theoretical analysis – characteristics and ill-posedness

Eqs. (1)–(4) form a system of 1st-order PDEs, and characteristic roots, λ, of the system can be found. The system is hyperbolic when the characteristic roots are real. Complex roots imply an elliptic system and cause the standard two-fluid model system to become ill-posed since only initial conditions can be specified in the temporal direction; under such a condition, any infinitesimal disturbance will cause the waves to grow exponentially without bound.

Let U be the vector $(\alpha_l,u_l,u_g,p)^{\mathrm{T}}$. Eqs. (1)–(4) can be written in vector form as

$$[A]\frac{\partial\mathbf{U}}{\partial t}+[B]\frac{\partial\mathbf{U}}{\partial x}=[C], \tag{11}$$

where $[A]$, $[B]$ and $[C]$ are coefficient matrices given by

$$[A]=\begin{bmatrix}1&0&0&0\\-1&0&0&0\\u_l&\alpha_l&0&0\\-u_g&0&\alpha_g&0\end{bmatrix}, \tag{12a}$$

$$[B]=\begin{bmatrix}u_l&\alpha_l&0&0\\-u_g&0&\alpha_g&0\\u_l^2+gH_l\cos\beta&2\alpha_l u_l&0&\frac{\alpha_l}{\rho_l}\\-u_g^2+gH_g\cos\beta&0&2\alpha_g u_g&\frac{\alpha_g}{\rho_g}\end{bmatrix}, \tag{12b}$$

$$[C]=\begin{bmatrix}0\\0\\-\alpha_l g\sin\beta-\frac{\tau_l S_l}{A\rho_l}+\frac{\tau_i S_i}{A\rho_l}\\-\alpha_g g\sin\beta-\frac{\tau_g S_g}{A\rho_g}-\frac{\tau_i S_i}{A\rho_g}\end{bmatrix}. \tag{12c}$$

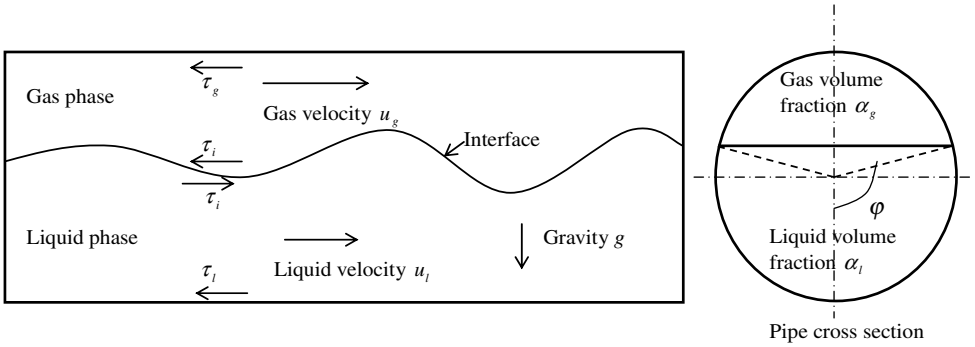

Fig. 1. Schematic depiction of two-phase flow in a horizontal pipe.

The characteristic roots λ of the system are determined from:

$$||[A]\lambda - [B]|| = 0, \tag{13}$$

where $||\ ||$ denotes the determinant of the matrix. After expansion of the above determinant, the characteristic roots are obtained,

$$\lambda = \frac{\left(\frac{\rho_l u_l}{\alpha_l} + \frac{\rho_g u_g}{\alpha_g}\right) \pm \sqrt{\left(\frac{\rho_l}{\alpha_l} + \frac{\rho_g}{\alpha_g}\right)\frac{\rho_l - \rho_g}{\alpha'_l} g\cos\beta - \frac{\rho_l \rho_g}{\alpha_l \alpha_g}(u_g - u_l)^2}}{\frac{\rho_l}{\alpha_l} + \frac{\rho_g}{\alpha_g}}. \tag{14}$$

When $g = 0$, Eq. (14) possesses real roots only if $\lambda = u_g = u_l$. Otherwise, the standard two-fluid model becomes ill-posed (Gidaspow, 1974). If $g \neq 0$, the real roots (or well-posedness) requirement gives

$$\Delta U^2 = (u_g - u_l)^2 < \Delta U_c^2 = \left(\frac{\alpha_l}{\rho_l} + \frac{\alpha_g}{\rho_g}\right)\frac{\rho_l - \rho_g}{\alpha'_l} g\cos\beta. \tag{15}$$

Eq. (15) gives the critical value ΔU_c for the slip velocity ΔU between two phases, beyond which the system becomes ill-posed. The ill-posedness criterion based on the characteristic analysis is exactly the same as that from the IKH analysis for the standard two-fluid model (Barnea and Taitel, 1994).

It is noted that the two fluid model viscous terms appear only in vector $[C]$. However, Eq. (13) shows that the characteristics are not affected by the vector $[C]$. Thus, viscous terms in the standard two-fluid model do not affect its characteristics. The criterion for ill-posedness for the standard viscous two-fluid model is identical to that for the standard inviscid two-fluid model.

Nevertheless, the viscous effect in $[C]$ can affect the linear stability of the standard two-fluid model. When an infinitesimal disturbance is introduced to a steady state base flow and the amplitude for a certain wavelength grows with time, the base flow condition is referred to as viscous Kelvin–Helmholtz (VKH) unstable. In the physical flow field, the amplitude grows to be order one and causes the flow regime to transition from stratified to slug flow (Issa and Kempf, 2003). Details of the VKH and IKH instability analyses can be found in Liao (2005).

The IKH analysis provides a stability condition for the standard two-fluid model as well as useful information on the growth rate of disturbances in the standard inviscid two-fluid model. Mass and momentum equations of the liquid phase and the gas phase are linearized and substituted for the perturbed liquid volume fraction, liquid and gas phase velocities, and pressure in the form of $\varepsilon \exp(I(\omega t - kx))$ in which $I = \sqrt{-1}$ denotes the imaginary unit, ε is the amplitude, ω is the angular frequency, and k is the wavenumber. The following system is obtained for the disturbance amplitude:

$$\begin{vmatrix} \omega - u_l k & -\alpha_l k & 0 & 0 \\ \omega - u_g k & 0 & \alpha_g k & 0 \\ -k\frac{H_l}{\alpha_l} g\cos\beta & \omega - u_l k & 0 & \frac{k}{\rho_l} \\ -k\frac{H_l}{\alpha_l} g\cos\beta & 0 & \omega - u_g k & \frac{k}{\rho_g} \end{vmatrix} \begin{vmatrix} \varepsilon \\ \varepsilon_l \\ \varepsilon_g \\ \varepsilon_p \end{vmatrix} = 0. \tag{16}$$

It is noted that the stability condition for IKH analysis obtained from Eq. (16) is identical to the ill-posedness condition. However, the stability condition of VKH is different from IKH and usually occurs at a lower slip velocity. The corresponding disturbance amplitude for VKH is given in Liao (2005). Eq. (16) also serves as a constraint on the amplitude and phase of the initial disturbances in the numerical simulation using the standard inviscid two-fluid model.

4. Computational instability analysis

4.1. Description of the numerical method

Since the shear stress terms in the standard two-fluid model are only source terms, they do not affect the ill-posedness as discussed in Section 3. For simplicity, numerical implementation for the standard inviscid two-fluid model is first introduced. The mass conservation equations are the same for the standard viscous and inviscid two-fluid models. The inviscid momentum conservation equations are Eqs. (3) and (4) without the shear stress terms.

In general, the governing Eqs. (1)–(4) without the shear stress terms are solved iteratively. The basic procedure is to solve the liquid continuity equation for the liquid volume fraction, and the liquid and gas phase momentum equations are used to obtain the liquid and gas phase velocities. To obtain a governing equation for the pressure, Eqs. (1) and (2) are first combined to form a total mass conservation,

$$\frac{\partial}{\partial x}(u_g \alpha_g) + \frac{\partial}{\partial x}(u_l \alpha_l) = 0. \tag{17}$$

Substituting the liquid and gas momentum equations into Eq. (17) yields a constraint on pressure. A SIMPLE type of pressure correction scheme (Patankar, 1980) is then used.

A finite volume method is employed to discretize the governing equations. A staggered grid (Fig. 2) is adopted to obtain a compact stencil for pressure (Ferziger and Peric, 1996). On the staggered grids, the flow properties such as volume fraction, density and pressure are evaluated at the center of the main control volume, and the liquid and gas velocities are evaluated at the cell face of the main control volume.

The Euler backward scheme is employed for the transient term. The discretized liquid continuity equation becomes

$$\frac{\Delta x}{\Delta t}((\alpha_l)_P - (\alpha_l)_P^0) + (\alpha_l u_l)_e - (\alpha_l u_l)_w = 0, \tag{18}$$

where the superscript 0 denotes the values at the previous time step. The subscript P denotes the center of the main control volume, while subscripts e and w denote the east and west faces of the main control volume, respectively. The liquid velocity at the cell face is known, and the volume fraction at the cell face is evaluated using various interpolation schemes. Among them, CD, FOU, SOU, and QUICK schemes are commonly used. Eq. (2) for the gas phase is similarly discretized.

The liquid momentum equation (Eq. (3) without shear stress terms) is integrated across the velocity control volume. Using similar notation, the discretized liquid momentum equation is

$$\frac{\Delta x}{\Delta t}\left((\alpha_l u_l)_P - (\alpha_l u_l)_P^0\right) + (u_l)_e(\alpha_l u_l)_e - (u_l)_w(\alpha_l u_l)_w = \frac{(\alpha_l)_P}{\rho_l}(p_w - p_e) + ((\alpha_l)_w - (\alpha_l)_e)H_l g\cos\beta - \Delta x(\alpha_l)_P g\sin\beta. \tag{19}$$

It is important to note that the interpolation schemes used in Eq. (19) must be exactly the same as those in Eq. (18) in order to reduce the dissipation and dispersion errors.

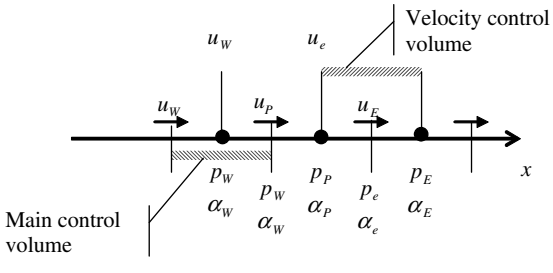

Fig. 2. Staggered grid arrangement in standard two-fluid model.

The gas phase momentum equation is similarly treated,

$$\frac{\Delta x}{\Delta t}\left((\alpha_g u_g)_P - (\alpha_g u_g)_P^0\right) + (u_g)_e(\alpha_g u_g)_e - (u_g)_w(\alpha_g u_g)_w = \frac{(\alpha_g)_P}{\rho_g}(p_w - p_e) + ((\alpha_l)_w - (\alpha_l)_e)H_g g\cos\beta - \Delta x(\alpha_g)_P g\sin\beta. \tag{20}$$

For the pressure correction scheme, Eq. (17) is integrated across the main control volume. The discretized equation is

$$(\alpha_g u_g)_e - (\alpha_g u_g)_w + (\alpha_l u_l)_e - (\alpha_l u_l)_w = 0. \tag{21}$$

Because Eq. (17) is obtained by combining Eqs. (1) and (2), the discretization of Eq. (21) should be exactly the same as that of Eq. (18) and discretized Eq. (2). The final pressure equation is obtained by substituting the two momentum Eqs. (19) and (20), into Eq. (21).

It is noted that the SOU scheme involves five grids points. However, this study only simulates uni-directional co-current flow, where the contribution of the downstream side grids is always zero in the discretized equation. The five point scheme in the discretized equations is reduced to a three point scheme. The final discretized 3 point equation is solved directly using the standard Thomas algorithm.

4.2. von Neumann analysis for various convection schemes

von Neumann stability analysis (Hirsch, 1988) is commonly used for analyzing the stability of a finite difference scheme. In this derivation, the FOU scheme is used as an example, and both liquid and gas velocities are assumed positive. The grid index is shown in Fig. 3. Discretization of Eq. (18) using FOU leads to

$$\frac{(\alpha_l)_i^n - (\alpha_l)_i^{n-1}}{\Delta t}\Delta x + \left((u_l)_{i+\frac{1}{2}}^n(\alpha_l)_i^n - (u_l)_{i-\frac{1}{2}}^n(\alpha_l)_{i-1}^n\right) = 0. \tag{22}$$

Splitting the variables into base values and disturbances, the linearized equation for the disturbance of α_l is

$$\frac{(\hat{\alpha}_l)_i^n - (\hat{\alpha}_l)_i^{n-1}}{\Delta t}\Delta x + \left(\alpha_l\left((\hat{u}_l)_{i+\frac{1}{2}}^n - (\hat{u}_l)_{i-\frac{1}{2}}^n\right) + u_l((\hat{\alpha}_l)_i^n - (\hat{\alpha}_l)_{i-1}^n)\right) = 0, \tag{23}$$

where "$\hat{}$" denotes disturbance values. Expressing disturbances as

$$(\hat{\alpha}_l)_i^n = \varepsilon E^n e^{Ikx}, \quad (\hat{u}_l)_i^n = \varepsilon_l E^n e^{Ikx}, \quad (\hat{u}_g)_i^n = \varepsilon_g E^n e^{Ikx}, \tag{24}$$

where E is a common amplitude factor, and k is the wavenumber, Eq. (23) is simplified to

$$\varepsilon\left(\frac{\Delta x}{\Delta t}(1 - G^{-1}) + u_l(1 - e^{-I\phi})\right) + \varepsilon_l\alpha_l\left(e^{\frac{1}{2}I\phi} - e^{-\frac{1}{2}I\phi}\right) = 0. \tag{25}$$

Here G is the amplification factor,

$$G = E^n/E^{n-1}, \tag{26}$$

and ϕ is the phase angle,

$$\phi = k\cdot\Delta x, \tag{27}$$

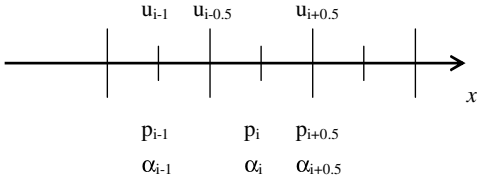

Fig. 3. Grid index in staggered grid for von Neumann stability analysis.

defined over $[0,\pi]$ and it represents all the resolvable wave components in the computational domain for the given grid. Short waves correspond to the region near $\phi = \pi$.

The wave growth equation for the gas phase mass conservation equation is similarly obtained,

$$\varepsilon\left(\frac{\Delta x}{\Delta t}(1 - G^{-1}) + u_g(1 - e^{-I\phi})\right) - \varepsilon_g\alpha_g\left(e^{\frac{1}{2}I\phi} - e^{-\frac{1}{2}I\phi}\right) = 0. \tag{28}$$

For the liquid momentum, Eq. (19) is discretized with the FOU scheme as

$$\frac{(u_l)_{i+\frac{1}{2}}^n(\alpha_l)_{i+\frac{1}{2}}^n - (u_l)_{i+\frac{1}{2}}^{n-1}(\alpha_l)_{i+\frac{1}{2}}^{n-1}}{\Delta t}\Delta x + ((u_l)_{i+1}^n(\alpha_l u_l)_{i+\frac{1}{2}}^n - (u_l)_i^n(\alpha_l u_l)_{i-\frac{1}{2}}^n) = \frac{(\alpha_l)_{i+\frac{1}{2}}^n}{\rho_l}((p)_i^n - (p)_{i+1}^n) + g\cos\beta H_l((\alpha_l)_i^n - (\alpha_l)_{i+1}^n) - \Delta x\rho_l(\alpha_l)_{i+\frac{1}{2}}^n g\sin\beta, \tag{29}$$

which is subsequently linearized and simplified with the aid of the liquid mass conservation equation,

$$\frac{\Delta x}{\Delta t}\left(\rho_l((\hat{u}_l)_{i+\frac{1}{2}}^n - (\hat{u}_l)_{i+\frac{1}{2}}^{n-1})\right) + \rho_l u_l((\hat{u}_l)_{i+\frac{1}{2}}^n - (\hat{u}_l)_{i-\frac{1}{2}}^n) = (\hat{p}_i^n - \hat{p}_{i+1}^n) + \rho_l g\cos\beta\frac{H_l}{\alpha_l}((\hat{\alpha}_l)_i^n - (\hat{\alpha}_l)_{i+1}^n). \tag{30}$$

For the gas phase, the velocity disturbance is governed by

$$\frac{\Delta x}{\Delta t}(\rho_g((\hat{u}_g)_{i+\frac{1}{2}}^n - (\hat{u}_g)_{i+\frac{1}{2}}^{n-1})) + \rho_g u_g((\hat{u}_g)_{i+\frac{1}{2}}^n - (\hat{u}_g)_{i-\frac{1}{2}}^n) = (\hat{p}_i^n - \hat{p}_{i+1}^n) + \rho_g g\cos\beta\frac{H_g}{\alpha_g}((\hat{\alpha}_l)_i^n - (\hat{\alpha}_l)_{i+1}^n). \tag{31}$$

The pressure term can be canceled by combining Eqs. (30) and (31). Substituting Eq. (24) into the combined momentum equation leads to

$$\varepsilon_l\left(\frac{\Delta x}{\Delta t}\rho_l(1 - G^{-1}) + \rho_l u_l(1 - e^{-I\phi})\right) - \varepsilon_g\left(\frac{\Delta x}{\Delta t}\rho_g(1 - G^{-1}) + \rho_g u_g(1 - e^{-I\phi})\right) + \varepsilon(\rho_l - \rho_g)g \times\cos\beta\frac{H_l}{\alpha_l}\left(e^{\frac{1}{2}I\phi} - e^{-\frac{1}{2}I\phi}\right) = 0. \tag{32}$$

Eqs. (25), (28) and (32) are written in the form of an amplification matrix:

$$\begin{bmatrix} \frac{\Delta x}{\Delta t}(1 - G^{-1}) + u_g(1 - e^{-I\phi}) & -\alpha_g\left(e^{\frac{1}{2}I\phi} - e^{-\frac{1}{2}I\phi}\right) & 0 \\ \frac{\Delta x}{\Delta t}(1 - G^{-1}) + u_l(1 - e^{-I\phi}) & 0 & \alpha_l\left(e^{\frac{1}{2}I\phi} - e^{-\frac{1}{2}I\phi}\right) \\ (\rho_l - \rho_g)g\cos\beta\frac{H_l}{\alpha_l}\left(e^{\frac{1}{2}I\phi} - e^{-\frac{1}{2}I\phi}\right) & -\rho_g\left(\frac{\Delta x}{\Delta t}(1 - G^{-1}) + u_g(1 - e^{-I\phi})\right) & \rho_l\left(\frac{\Delta x}{\Delta t}(1 - G^{-1}) + u_l(1 - e^{-I\phi})\right) \end{bmatrix}\begin{vmatrix} \varepsilon \\ \varepsilon_g \\ \varepsilon_l \end{vmatrix} = 0. \tag{33}$$

Non-trivial solutions for $(\varepsilon, \varepsilon_g, \varepsilon_l)^T$ exist only when the determinant of the matrix is zero. Hence,

$$a(G^{-1})^2 + b(G^{-1}) + c = 0, \tag{34}$$

where

$$a = \frac{\rho_l}{\alpha_l} + \frac{\rho_g}{\alpha_g}, \tag{35a}$$

$$b = -2\left(\frac{\rho_g}{\alpha_g}(1 + CFL_g\Delta(\phi)) + \frac{\rho_l}{\alpha_l}(1 + CFL_l\Delta(\phi))\right), \tag{35b}$$

$$c = \frac{\rho_g}{\alpha_g}(1 + CFL_g\Delta(\phi))^2 + \frac{\rho_l}{\alpha_l}(1 + CFL_l\Delta(\phi))^2 + \left(\frac{\Delta t}{\Delta x}\right)^2(\rho_l - \rho_g)g\cos\beta\frac{H_l}{\alpha_l}\left(4\sin^2\left(\frac{\phi}{2}\right)\right), \tag{35c}$$

and $\Delta(\phi) = 1 - e^{-I\phi}$, CFL is the Courant number,

$$CFL_l = \frac{\Delta t}{\Delta x}u_l, \text{and } CFL_g = \frac{\Delta t}{\Delta x}u_g. \tag{36}$$

Eq. (34) is valid for the amplification factor of other discretization schemes with appropriate $\Delta(\phi)$. The values of $\Delta(\phi)$ for different schemes are summarized in Table 1. The amplification factors can be easily found from Eq. (34),

$$G = \frac{2a}{-b \pm \sqrt{b^2 - 4ac}}. \tag{37}$$

The scheme will be stable when the spectral radius $\rho(G) \leqslant 1$ for all ϕ.

4.3. Numerical scheme and von Neumann stability analysis for the standard viscous two-fluid model

The pressure correction scheme for the inviscid two-fluid model in Section 4.1 can be extended to solve the standard viscous two-fluid model with inclusion of the wall friction and interfacial drag terms.

Generally, the von Neumann stability analysis for the standard viscous two-fluid model scheme is similar to that for the standard inviscid two-fluid model. Both the liquid and gas velocities are assumed positive for simplicity and practicality.

The equation for the amplification factor G shares the same form as that for the inviscid two-fluid model growth rate equation (Eq. (34)) but with different coefficients:

$$a = \frac{\rho_l}{\alpha_l} + \frac{\rho_g}{\alpha_g}, \tag{38a}$$

$$b = -2\left(\frac{\rho_g}{\alpha_g}(1 + CFL_g\Delta(\phi)) + \frac{\rho_l}{\alpha_l}(1 + CFL_l\Delta(\phi))\right) + \Delta t\left(\frac{1}{\alpha_g}\frac{\partial F}{\partial u_g} - \frac{1}{\alpha_l}\frac{\partial F}{\partial u_l}\right), \tag{38b}$$

$$c = \frac{\rho_g}{\alpha_g}(1 + CFL_g\Delta(\phi))^2 + \frac{\rho_l}{\alpha_l}(1 + CFL_l\Delta(\phi))^2 + \left(\frac{\Delta t}{\Delta x}\right)^2(\rho_l - \rho_g)g\cos\beta\frac{H_l}{\alpha_l}\left(4\sin^2\left(\frac{\phi}{2}\right)\right) + I\left(\frac{\Delta t}{\Delta x}\right)\Delta t\sin\phi\frac{\partial F}{\partial \alpha_l} + \frac{\Delta t}{\alpha_g}\frac{\partial F}{\partial u_g}(1 + CFL_g\Delta(\phi)) - \frac{\Delta t}{\alpha_l}\frac{\partial F}{\partial u_l}(1 + CFL_l\Delta(\phi)), \tag{38c}$$

Table 1
$\Delta(\phi)$ for different discretization schemes

Scheme	$\Delta(\phi)$
1st-order upwind	$1-e^{-I\phi}$
Central difference	$\frac{e^{I\phi}-e^{-I\phi}}{2}$
2nd-order upwind	$\frac{3-4e^{-I\phi}+e^{-2I\phi}}{2}$
QUICK	$\frac{3e^{I\phi}+3-7e^{-I\phi}+e^{-2I\phi}}{8}$

where

$$F = F_l + F_g, \tag{39}$$

and

$$F_l = -\frac{\tau_l S_l}{A\alpha_l} + \frac{\tau_i S_i}{A\alpha_l} - \rho_l g\sin\beta, \tag{40}$$

$$F_g = -\frac{\tau_g S_g}{A\alpha_g} - \frac{\tau_i S_i}{A\alpha_g} - \rho_g g\sin\beta. \tag{41}$$

The values of $\Delta(\phi)$ in Eq. (38) are summarized in Table 1. Comparing the amplification factor of the standard inviscid two-fluid model (Eqs. (35)a–c), with that for the standard viscous two-fluid model (Eqs. (38)a–c) additional terms representing the influence of wall shear stress and interfacial stress on G are readily observable.

4.4. Initial and boundary conditions for numerical solutions

With von Neumann stability analysis, a periodic boundary condition is implicitly assumed. In the computations, such periodic boundary conditions are necessarily employed in order to provide a direct comparison.

The von Neumann stability analysis tracks the growth of an infinitesimal disturbance. In computations, a small initial disturbance must be properly introduced without generating additional higher order harmonic noise. The best initial condition for the disturbance is that from the wave growth equation, such as given by Eq. (33) for the FOU scheme. However, this approach makes the imposition of the initial condition too complicated, since initial conditions vary from one numerical scheme to another. A simpler, yet effective approach is to use the solution from inviscid Kelvin–Helmholtz analysis. When the wavenumber of a small amplitude primary disturbance, k_0, is specified at $t = 0$, the corresponding value for ω can be obtained by setting the determinant of the matrix in Eq. (16) to zero. Upon the specification of ε_l the rest of the complex valued amplitudes, such as $\varepsilon = \frac{\alpha_l}{\frac{\omega}{k} - u_l}\varepsilon_l$, and similar expressions for ε_g, and ε_p can be determined from Eq. (16). An initial condition describing a small amplitude primary disturbance that is consistent with the governing equations is important for quantitatively studying the growth of the disturbance in the context of the standard two-fluid model. Should the initial condition be inconsistent with the original equations, unexpected higher harmonic wave components may develop immediately after the computation is initiated. Since the flow condition under consideration is close to becoming unstable, such an additional disturbance may grow and overtake the targeted primary disturbance and makes it difficult to assess the accuracy of the numerical scheme.

5. Results and discussion

5.1. Computational stability assessment based on von Neumann stability analysis

It is well known that for ordinary convection–diffusion equations, the FOU scheme is less accurate due to the high level of numerical diffusion. The higher order schemes, such as SOU, CD, and QUICK, on the other hand, have lower numerical diffusion and should be more accurate. It is also well known that the CD scheme is prone to generate grid scale (high wavenumber) oscillations, which often lead to numerical instability in highly non-linear systems. To gain an insight into the performance of various discretization schemes when they are applied to the standard two-fluid model system, detailed comparisons of stability characteristics of the FOU, SOU, CD, and QUICK schemes on the standard inviscid two-fluid model are presented first for flow conditions before, near, and after the ill-posedness. Numerical solutions after ill-posedness are NOT to be construed to possess physical meaning,

but instead are useful in understanding the growth of the targeted primary disturbance, selection of the wavelength of the emerging short waves, and the growth of those short waves when various discretization schemes are used.

In this study, air/water stratified flow in a round pipe is considered. The densities of water and air are 1000 and 1.1614 kg/m^3, respectively. The pipe diameter is 0.078 m and the inclination angle is $\beta = 0$. For the unperturbed base flow, the following is used: $\alpha_l = 0.5$, $u_l = 1$ m/s, $u_g = 17$ m/s. The pipe diameter for the inviscid flow calculation is $D = 0.078$ m for the discussions presented in Sections 5.1–5.5, while the pipe diameter used for the viscous flow instability analysis in Section 5.6 is $D = 0.05$ m. The *CFL* number based on the liquid velocity u_l is 0.1. The IKH stability condition, based on Eq. (15) for the above parameters, is satisfied since $\Delta U = 16$ m/s $< \Delta U_c = 16.0768$ m/s. Thus, the standard two-fluid model for the present condition is analytically well-posed. However, since the slip velocity is so close to the ill-posed threshold value, it serves as an ideal testing case to assess the performance of various discretization schemes. There are two values of G given by Eq. (37). Since the one with larger magnitude determines the instability, only the larger $|G|$ is used in this study.

Fig. 4 compares the amplification factors $|G(\phi)|$, in which $\phi = k\Delta x$, of four discretization schemes. The solid line is the amplification factor by IKH analysis with $G = 1$ for a well-posed hyperbolic system. The dashed line is that for the CD scheme. It is slightly lower than one, but is very close to one with a slight diffusion error in the high wavenumber range. This implies the CD scheme is ideal for computing the standard two-fluid model. The amplification factor for the FOU scheme shows excessive numerical diffusion at high k. Furthermore, $|G| > 1$ at low k, and the computation using FOU is unstable at this flow condition despite the excessive level of numerical diffusion. Although SOU is often regarded as a better scheme than FOU with less numerical diffusion, its performance in the standard two-fluid model is very poor. For large k, the numerical diffusion of SOU is much larger than that of FOU. For small k, the amplification factor of SOU is much larger than that of FOU. The dashed-dot line is the amplification factor of the QUICK scheme. Its numerical damping at high k is lower than that of FOU and SOU schemes, but it is still much larger than that of the CD scheme. At small k, $|G|$ being slightly larger than one indicates that QUICK is unstable as well. The reason that the amplification factor of the CD scheme is close to the analytical amplification factor is due to the lack of 2nd-order diffusion error and low dispersion error. The overall performance of the SOU is worse than that of the FOU scheme: (a) $|G|$ exceeds unity further at lower k implying a stronger instability; (b) $|G|$ is far less than unity at higher k implying a higher damping for shorter waves. This suggests that the diffusion and dispersion error in the standard two-fluid model plays a much more complicated, and perhaps more negative, role on the numerical stability than that in the simple convection–diffusion equation. The interpolation scheme used in QUICK is essentially a linear interpolation with the upwind correction. Therefore its numerical damping and stability are worse than those of the CD scheme, but better than those of FOU and SOU schemes.

Another useful comparison among various discretization schemes can be made by examining the phase angle of the amplification factor, arg(G), which characterizes the extent of the numerical dispersion of a numerical scheme. Fig. 5 shows arg(G) of the amplification factors with larger absolute value; the unit of the phase angle is radians. It is seen that the dispersion of the CD scheme is smaller than the other 3 schemes. The SOU scheme has the largest dispersion error. The dispersion error of QUICK and FOU are comparable; and they are between the dispersion error of the CD and SOU schemes.

Next, the effect of the slip velocity $\Delta U = u_g - u_l$ on the numerical stability is examined. Fig. 6 shows the amplification factors of the CD scheme for a range of values of ΔU. When ΔU is smaller than the critical value, ΔU_c given by the von Neumann stability analysis, the magnitude of the amplification factors of all the harmonics in the computational domain are less than one. However, when $\Delta U > \Delta U_c$, $|G|$ in the low k range exceeds one, as shown by the curve for $\Delta U = 16.1$ m/s in Fig. 6. For the condition used in Fig. 6, numerical computations show a neutral stability condition for the CD scheme near $\Delta U_{c,\ CD} = 16.0773$ m/s, which is very close to $\Delta U_{c,\ IKH} = 16.0768$ m/s with an error of 0.003%. As ΔU further increases, $|G|$ increases as well. The range of unstable harmonic wavenumber becomes wider. The amplification factor of the CD scheme matches that of IKH only for very small k. In the high k range, numerical damping causes $|G|$ to depart from one more than in the intermediate k range.

Fig. 7 shows the amplification factors of the FOU scheme for different values of ΔU. The neutral or critical slip velocity for the

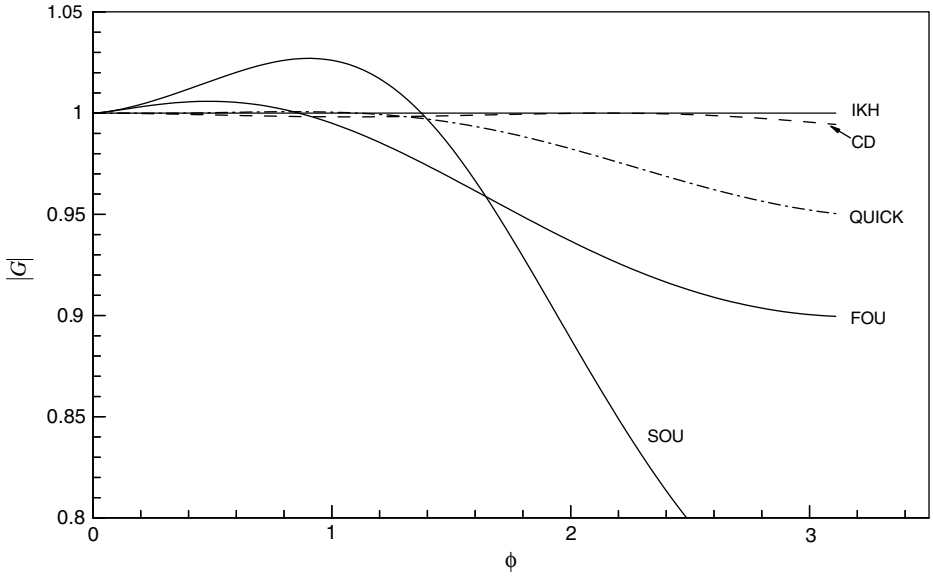

Fig. 4. Amplification factors of various numerical schemes for $N = 200$, $\alpha_l = 0.5$, $u_l = 1$ m/s, $u_g = 17$ m/s and $CFL_l = 0.1$.

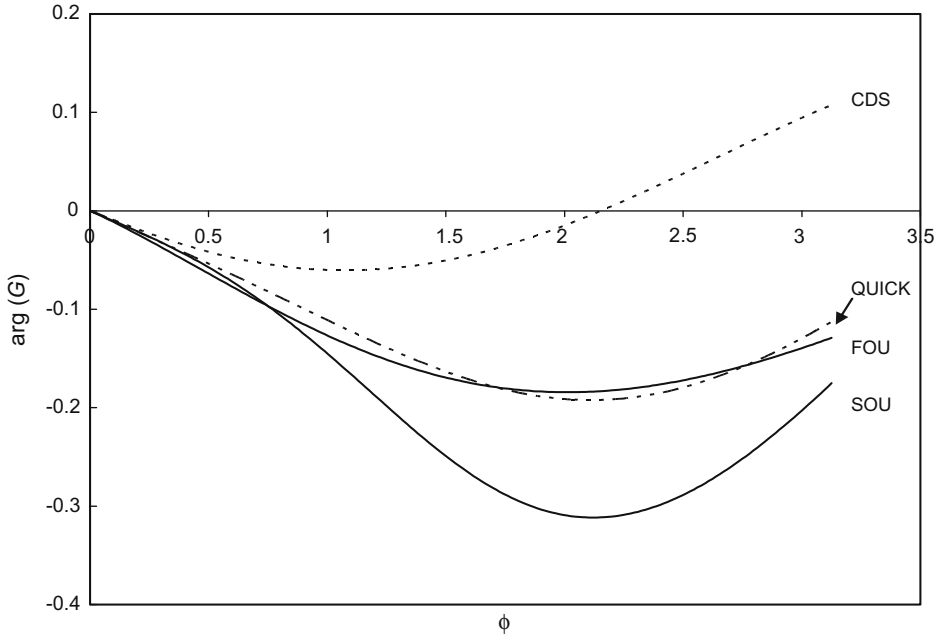

Fig. 5. Phase angle of the amplification factors with various numerical schemes for $N = 200$, $\alpha_l = 0.5$, $u_l = 1$ m/s, $u_g = 17$ m/s and $CFL_l = 0.1$. The unit of the phase angle is radians.

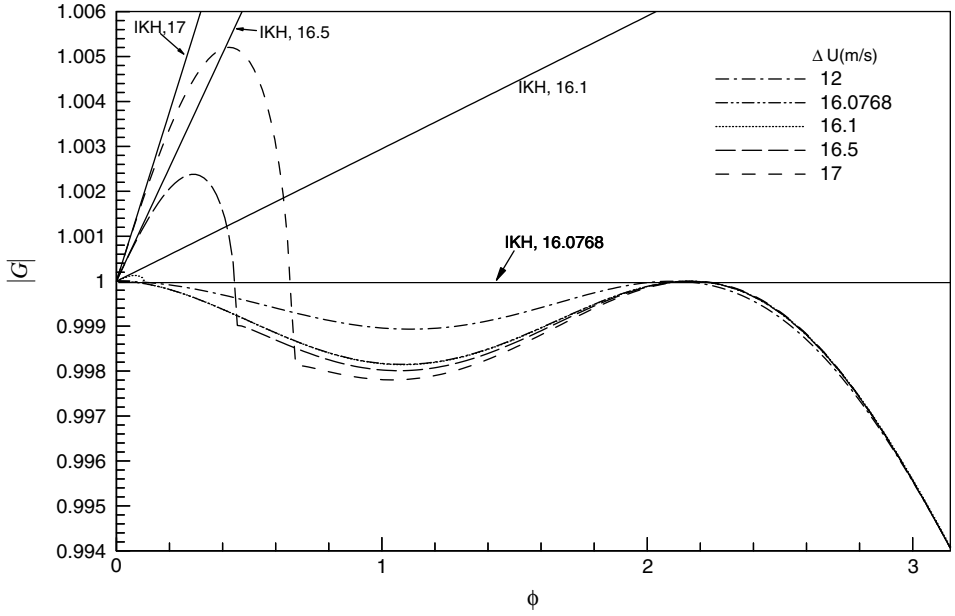

Fig. 6. Amplification factors of CD scheme with different values of ΔU for $N = 200$, $\alpha_l = 0.5$, $u_l = 1$ m/s, and $CFL_l = 0.1$.

stability conditions of SOU and QUICK schemes are $\Delta U_{c,SOU} = 13.73$ m/s and $\Delta U_{c,QUICK} = 16.03$ m/s, respectively. Unlike the CD scheme, there is no significant change of $|G|$ when ΔU varies. Numerical results from solving the governing equations indicate that the neutral stability for the condition shown in Fig. 7 is $\Delta U_{c,FOU} = 14.772$ m/s, which is significantly lower than the analytical value of $\Delta U_{c,IKH} = 16.0768$ m/s. The behavior of the SOU and QUICK schemes is similar to that of the FOU scheme, although for the sake of brevity similar graphs are not shown.

Fig. 8 shows the effect of the liquid velocity on the amplification factors of the CD scheme by keeping $\Delta U = 16$ m/s and $\Delta t/\Delta x = 0.1$ s/m constant. For $u_l = 0.01$ m/s and $u_l = 0.1$ m/s, $|G|$ decreases monotonically with $\phi = k\Delta x$ and noticeable damping at high k. When u_l increases, $|G|$ in high k range rises significantly, leaving a high damping saddle at the intermediate k range. On the other hand, when u_l is small and ΔU is kept constant, CFL_g/CFL_l is much larger than one so that it is difficult to keep both CFL_l and CFL_g in the moderate range, which is essential to the computational stability.

Fig. 9 shows the effect of u_l on $|G|$ for the FOU scheme with $\Delta U = 16$ m/s, $\Delta t/\Delta x = 0.1$ s/m. The behavior of FOU is quite different from that of CD shown in Fig. 8. When u_l is small, most harmonics are unstable because $\Delta U = 16$ m/s is very close to the IKH critical value for small u_l. However, for a larger u_l, excessive numerical diffusion present in the FOU scheme stabilizes the computations.

Figs. 10 and 11 show the effect of $\Delta t/\Delta x$ on $|G|$ for the CD and FOU schemes. There is increasing numerical diffusion with increas-

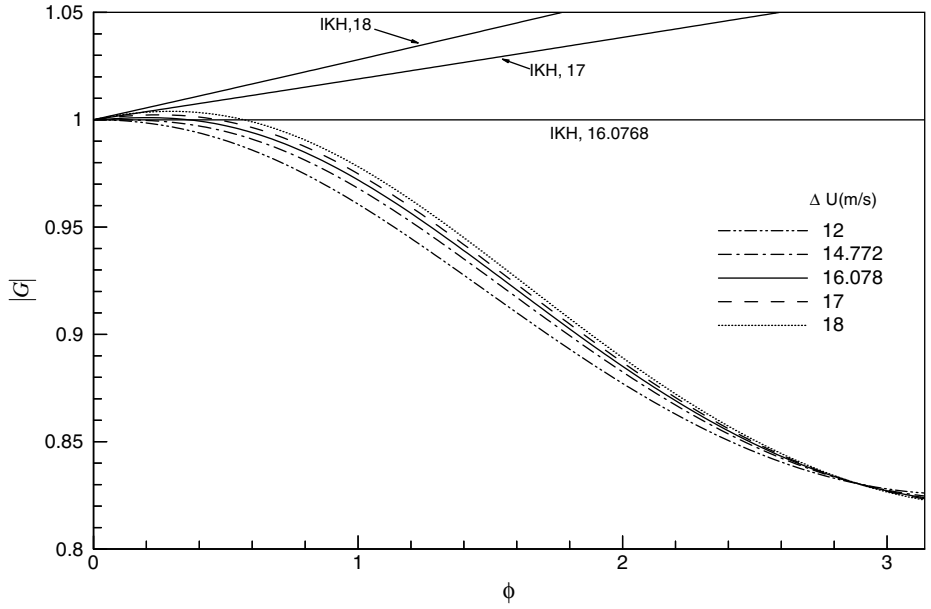

Fig. 7. Amplification factors of FOU scheme with different values of ΔU for $N = 200$, $\alpha_l = 0.5$, $u_l = 1$ m/s, and $CFL_l = 0.1$.

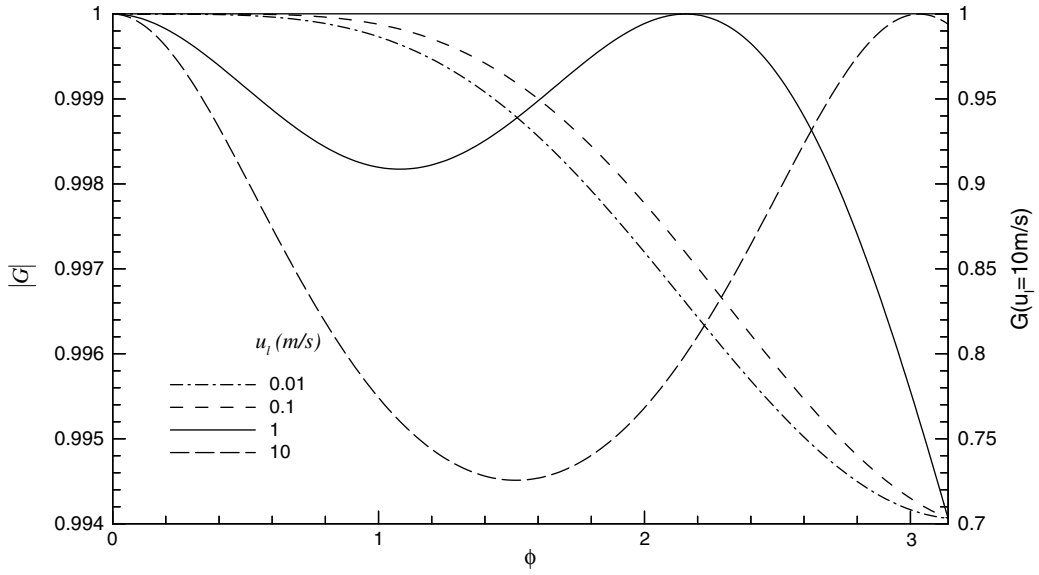

Fig. 8. Amplification factors of CD scheme with different values of u_l for $N = 200$, $\Delta U = 16$ m/s, $\alpha_l = 0.5$, and $\Delta t/\Delta x = 0.1$ s/m.

ing $\Delta t/\Delta x$, resulting in a decrease in $|G|$ for all wavenumbers. This can be explained by examining Eqs. (39)a–c. The only place where $\Delta t/\Delta x$ appears is in the last term for c, where it is multiplied by $(\rho_l - \rho_g)g$, which is known to stabilize stratified flow. Thus increasing $\Delta t/\Delta x$ enhances computational stability.

5.2. Consistency test

Consistency of a numerical scheme requires that the discretized equations approach the differential equations as the grid spacing Δx and time step Δt tend to zero (Hirsch, 1988). In other words, the truncation error must approach zero as $(\Delta x, \Delta t) \to 0$ for the Taylor series expansion to be valid.

To examine the consistency of the numerical scheme, growth rates with a small amplitude, sinusoidal primary disturbance and wavenumber $k_0 = 2\pi$ m^{-1} are obtained for different grid densities ($N = 100$, 200, and 400). The base flow is well-posed: $u_l = 1.0$ m/s, $u_g = 17.0$ m/s, $\beta = 0$, and $a_l = 0.5$. The computational domain is taken to be 1 m long so that $\Delta x = 0.01$, 0.005, and 0.0025. At $t = 0$ s, the initial disturbance is introduced such that Eq. (16) is satisfied. Consequently, $\omega = 6.735$ s^{-1}, and $\widehat{\alpha}_g(x) = \varepsilon\cos(k_0 x)$, where $\varepsilon = 6.366 \times 10^{-6}$. The rest of the flow variables are: $\hat{u}_g(x) = \varepsilon_g \cos(k_0 x)$ with $\varepsilon_g = 2.028 \times 10^{-4}$ m/s, and $\hat{u}_l(x) = \varepsilon_l \cos(k_0 x)$ with $\varepsilon_l = 9.165 \times 10^{-7}$ m/s.

Fig. 12 shows the computational error at $t = 1.5$ s obtained using the CD scheme for $N = 100$, 200, and 400. Computational error in this study is defined as,

$$Error = \sqrt{\frac{\sum_{i=1}^{N}\left[\left(\frac{u_l - u_{l,IKH}}{\varepsilon_l}\right)^2 + \left(\frac{u_g - u_{g,IKH}}{\varepsilon_g}\right)^2 + \left(\frac{\alpha_l - \alpha_{l,IKH}}{\varepsilon}\right)^2\right]}{N}}. \quad (41)$$

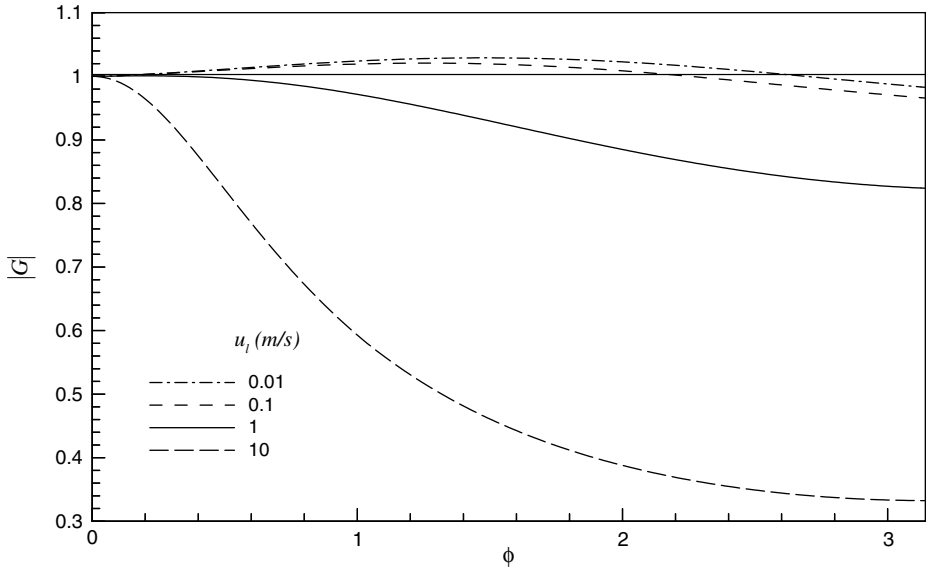

Fig. 9. Amplification factors of FOU scheme with different values of u_l for $N = 200$, $\Delta U = 16$ m/s, $\alpha_l = 0.5$, and $\Delta t/\Delta x = 0.1$ s/m.

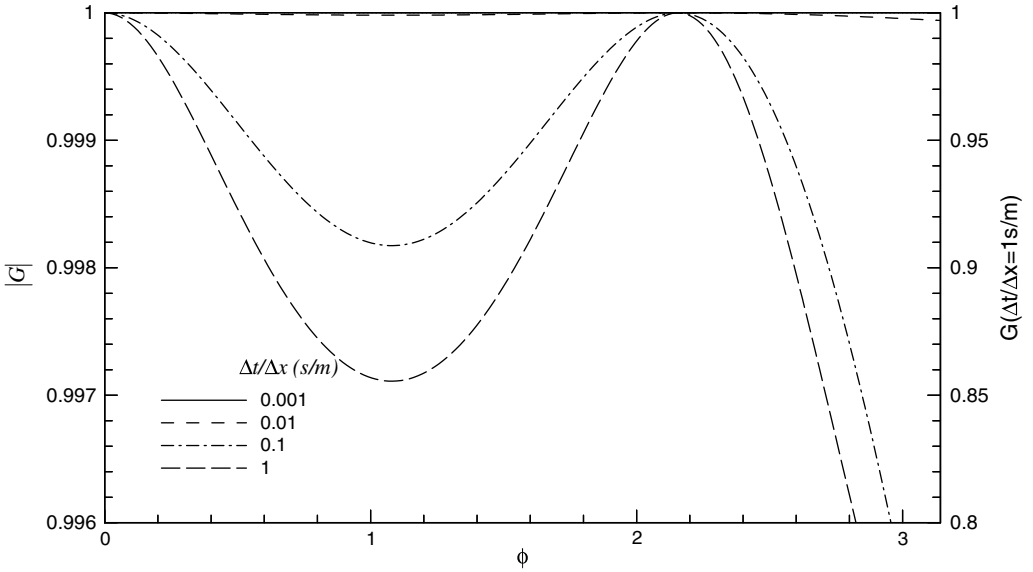

Fig. 10. Amplification factors of CD scheme with different values of $\Delta t/\Delta x$ for $N = 200$, $u_l = 1$ m/s, $\Delta U = 16$ m/s, and $\alpha_l = 0.5$.

The exact values used are from the analytical solution for $\widehat{\alpha}_g(x)$, $\widehat{u}_g(x)$, and $\hat{u}_l(x)$ given by the IKH analysis. The liquid CFL number is fixed at $CFL_l = 0.1$ for all three grids. Because CFL, u_l and u_g are constant in this comparison, $\Delta t/\Delta x$ is fixed. This ensures that Δt goes to zero as Δx approaches zero. With N increasing from 100 to 400, the error between the exact and numerical solutions decreases as required by consistency. Since the maximum normalized computational error is 0.0233 for $N = 200$ at $t = 1.5$ s, it is seen that $N = 200$ is sufficient for accurately capturing the disturbance wave with $k_0 = 2\pi\ \mathrm{m}^{-1}$. Hence it is used in the rest of this study unless otherwise mentioned. For FOU, SOU, and QUICK schemes, similar consistency behavior is observed when the computations are stable. For brevity, the graphical representation is not included.

5.3. Accuracy assessment based on the growth of disturbance

To further validate the accuracy of the pressure correction scheme, comparisons for the growth of the primary disturbance of $k_0 = 2\pi\ \mathrm{m}^{-1}$ between that computed and that predicted analytically using von Neumann stability analysis are presented. The base flow under consideration is: $u_l = 1$ m/s, $u_g = 15$ m/s, and $a_l = 0.5$. Hence based on IKH analysis, the disturbance does not grow with time. Fig. 13 shows the liquid velocity disturbance $\hat{u}_l(x)$ at $t = 4$ s after 16,000 time steps obtained using the CD scheme with $CFL_l = 0.05$. The amplitude of the computed $\hat{u}_l(x)$ is slightly smaller than that of the analytical solution from IKH analysis. The phases of the analytical and numerical solutions are almost identical. This demonstrates excellent performance of the CD scheme for the standard two-fluid model.

Further insight on the accuracy of the numerical scheme can be gained by examining the decay of the amplitude of $\hat{u}_l(x)$ using the amplification factor G obtained from the von Neumann analysis. For the present condition, the magnitude of the amplification factor of the CD scheme, with $k_0 = 2\pi\ \mathrm{m}^{-1}$, is $G = 0.999997962$ for each time step. Since it takes 16,000 steps to reach $t = 4$ s, the ratio of the disturbance amplitude at $t = 4$ s to that $t = 0$ s is

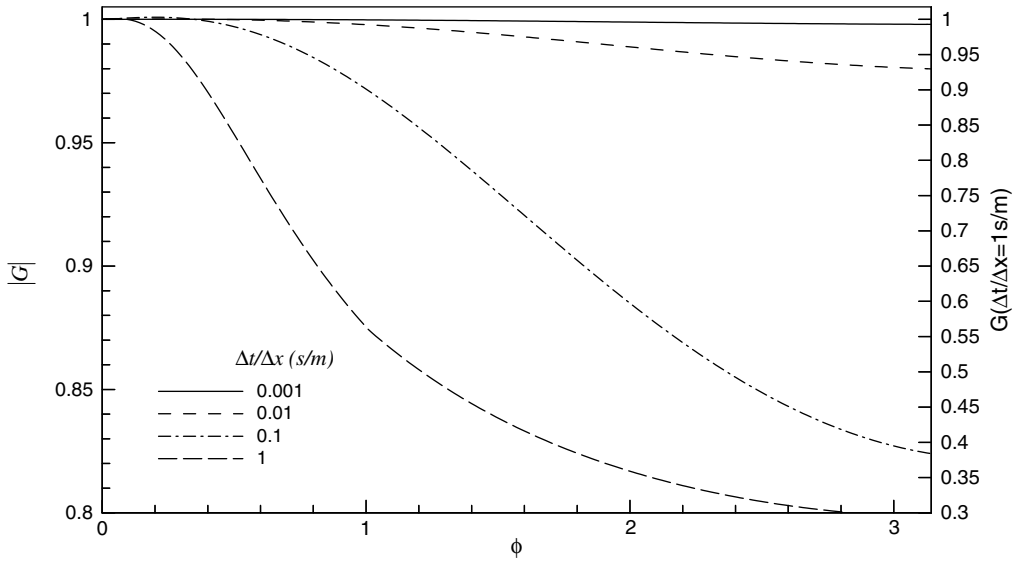

Fig. 11. Amplification factors of FOU scheme with different values of $\Delta t/\Delta x$ for $N = 200$, $u_l = 1$ m/s, $\Delta U = 16$ m/s, and $\alpha_l = 0.5$.

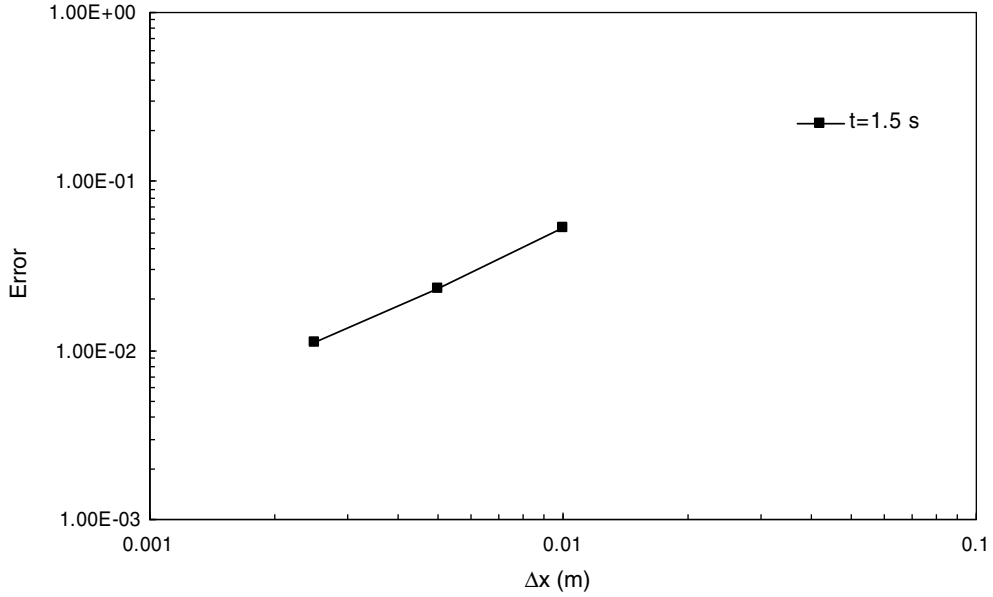

Fig. 12. Consistency test using different grid size with CD scheme for $u_l = 1$ m/s, $\Delta U = 16.5$ m/s (well-posed), $CFL_l = 0.1$, and $\alpha_l = 0.5$.

$(0.999997962)^{16{,}000} = 0.967918$. The actual ratio of the amplitude using CD scheme is 0.96807, with a difference of 0.016% in the ratios.

Fig. 14 shows the disturbance wave $\hat{u}_l(x)$ at $t = 4$ s (after 8000 time steps) and 5.2 s (after 10,400 time steps) for $u_l = 1$ m/s, $u_g = 17.5$ m/s, $a_l = 0.5$, and $CFL_l = 0.1$ using the CD scheme. The initial primary sinusoidal disturbance is introduced with $k_0 = 2\pi\ \mathrm{m}^{-1}$, $\alpha_g(x) = 6.366 \times 10^{-6}\cos(k_0 x)$, $\widehat{u}_1(x) = 2.437 \times 10^{-7}\cos(k_0 x) - 1.609 \times 10^{-6}\sin(k_0 x)$ m/s, and $\hat{u}_g(x) = 2.098 \times 10^{-4}\cos(\mathrm{k}_0 x) - 1.609 \times 10^{-6}\sin(\mathrm{k}_0 x)$ m/s. The slip velocity is $\Delta U = 16.5$ m/s which is larger than both the 16.0768 m/s threshold value from IKH analysis and 16.0773 m/s threshold value from the neutral stability condition of the von Neumann analysis. Hence, analytically it is ill-posed and computationally it is eventually unstable. Any perturbation should grow with time both analytically and computationally. At $t = 4$ s, $\hat{u}_l(x)$ is still sinusoidal with $k = k_0 = 2\pi\ \mathrm{m}^{-1}$. At $t = 5.2$ s, the original primary wave of $k_0 = 2\pi\ \mathrm{m}^{-1}$ is overwhelmed by a much stronger short wave. In Fig. 15, the growth history of the amplitude of $\hat{u}_l(x)$ is presented. The initial growth stage, from 0 to 4 s, corresponds to the growth of the initial primary wave with $k_0 = 2\pi\ \mathrm{m}^{-1}$. Using the von Neumann analysis for $|G(k = 2\pi\ \mathrm{m}^{-1})|$ the amplitude ratio between $t = 0$ and $t = 4$ s is 22.84, and the corresponding amplitude ratio from the computation using the CD scheme is 22.89, suggesting that the growth of the disturbance is dominated by the primary wave of $k_0 = 2\pi\ \mathrm{m}^{-1}$. After the initial growth stage a short wave with higher $|G|$ takes over and becomes dominant in the numerical solution. This corresponds to the stage of fast growth in Fig. 15. Although the amplitude of the short wave may not be considered as small anymore for the linear stability analysis to be perfectly valid, the wavenumber of the dominant short wave shown in Fig. 14 actually matches the one predicted by using the von Neumann analysis. For $\Delta U = 16$ m/s in the present computation, the highest $|G|$ occurs at $\phi_{\max} = k_{\max}\Delta x = 0.282743$ or $k_{\max} = \phi_{\max}/\Delta x = N\phi_{\max}$ for a 1 m long domain. This implies that

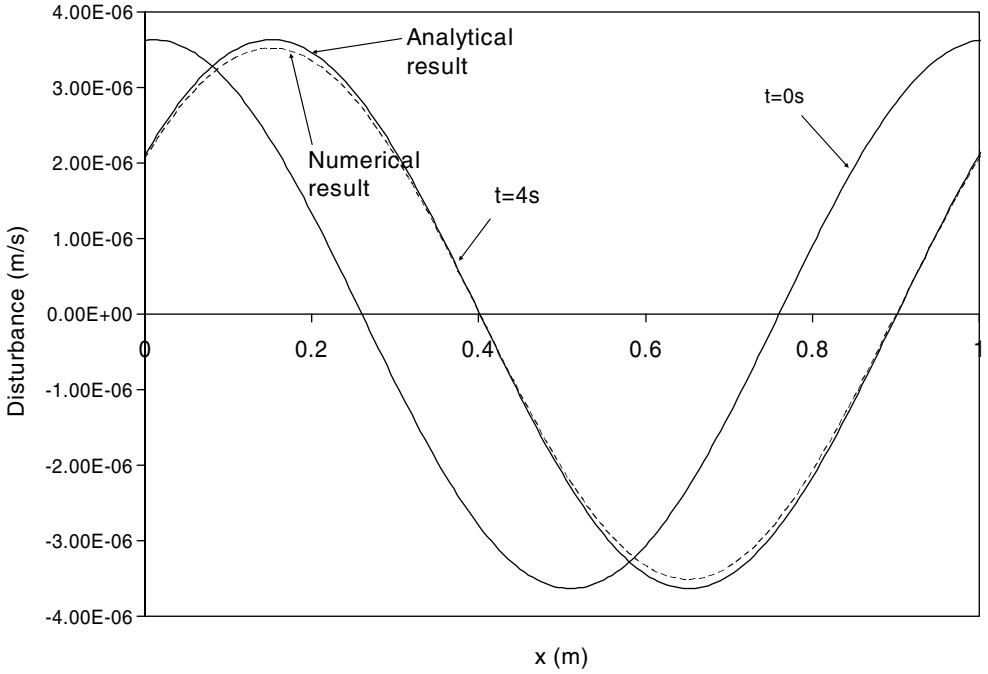

Fig. 13. Propagation of $\hat{u}_l$ using CD scheme for $N = 200$, $u_l = 1$ m/s, $\Delta U = 14$ m/s (well-posed), $CFL_l = 0.05$, $\alpha_l = 0.5$.

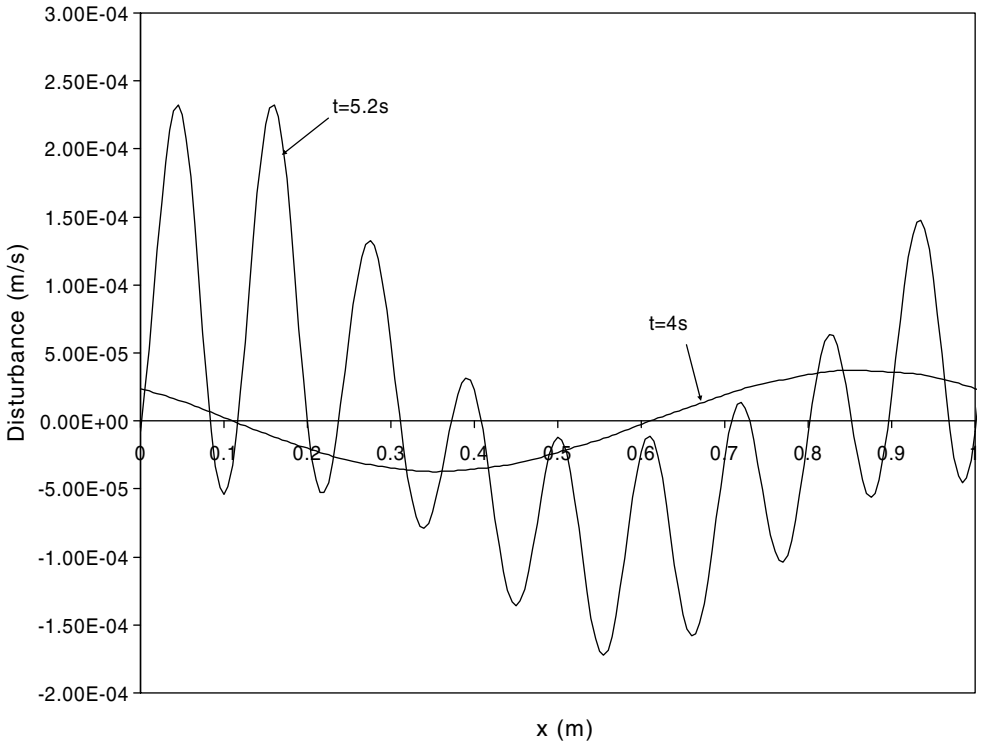

Fig. 14. Liquid velocity disturbance $\hat{u}_l$ after 10,400 time steps using CD scheme for $N = 200$, $u_l = 1$ m/s, $\Delta U = 16.5$ m/s (ill-posed), $CFL_l = 0.1$, $\alpha_l = 0.5$, and $t = 5.2$ s.

there should roughly be a total of $n = k_{max}/(2\pi) = N\phi_{max}/(2\pi) = 9$ peak-to-peak counts in the domain, which is the case shown in Fig. 14.

Next, a comparison between results from the FOU scheme and predictions from the von Neumann analysis is presented. The flow condition and computational parameters are: $u_l = 0.5$ m/s, $\Delta U = 16$ m/s, $a_l = 0.5$, $\beta = 0$; $N = 200$, and $CFL_l = 0.02$. The initial conditions for the primary disturbance are: $k_0 = 2\pi$ m^{-1}, $\varepsilon = 6.366 \times 10^{-6}$, $\varepsilon_l = 9.165 \times 10^{-7}$ m/s, and $\varepsilon_g = 2.028 \times 10^{-4}$ m/s. The flow is stable based on IKH stability analysis, but the computation will be unstable since for the FOU scheme $|G(\phi)| > 1$ for $0 < \phi = k\Delta x < 1.0210$ based on the von Neumann stability analysis, as shown in Fig. 16. The highest amplification factor is $|G|_{max} = 1.002014$ which occurs at $\phi_{max} = k_{max}\,\Delta x = 0.596902$. This gives $n = N\phi_{max}/(2\pi) = 19$. It is postulated that the harmonic wave with $k = k_{max}$ grows from the machine roundoff error at a rate of

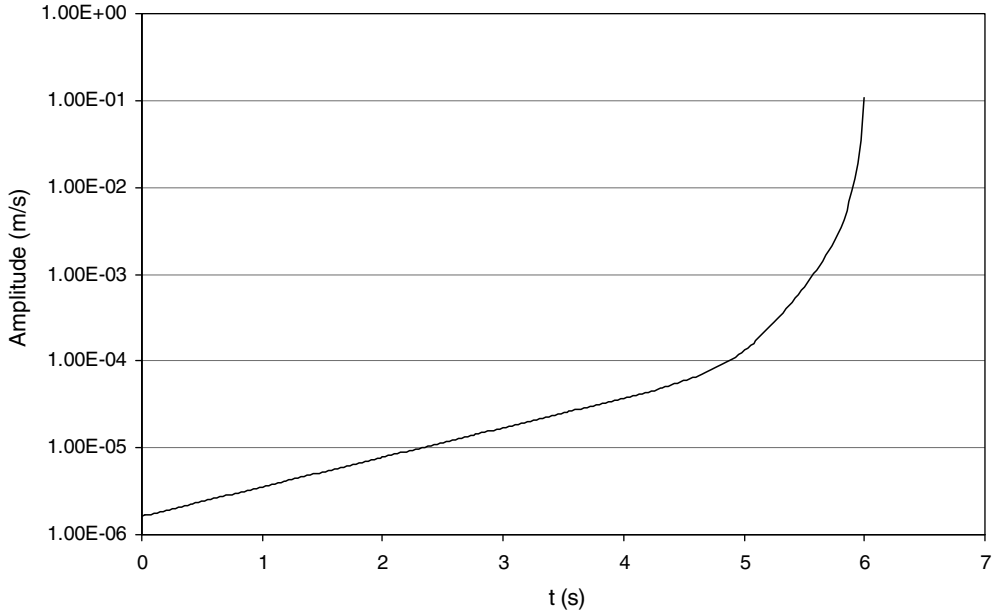

Fig. 15. Amplitude growth history of the liquid velocity disturbance $\hat{u}_l$ in Fig. 14.

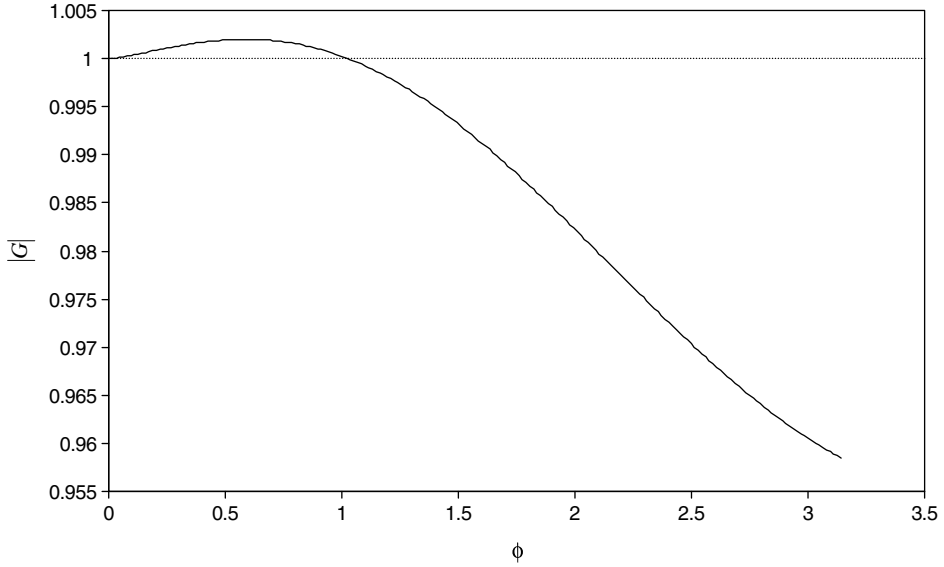

Fig. 16. Amplification factor of FOU scheme for $N = 200$, $u_l = 0.5$ m/s, $\Delta U = 16$ m/s, $CFL_l = 0.02$, and $\alpha_l = 0.5$.

1.002014 per time step and eventually dominates the targeted primary long wave disturbance of $k_0 = 2\pi\ \mathrm{m}^{-1}$ introduced at $t = 0$. Fig. 17 shows the $\hat{u}_l(x)$ after 12,000 time steps. For $k_0 = 2\pi m^{-1}$, $|G(0.0314)| = 1.00006270$ so that the amplitude of the primary disturbance will be $1.00006270^{12{,}000} = 2.122$ times the initial value. Clearly, short waves have grown to be as large as the primary wave component at $t = 2.4$. The peak-to-peak count of the short wave in Fig. 17 is 19 which matches $n = 19$ predicted using von Neumann analysis. Because the short waves originate from machine level error, which has a broad spectral distribution, the amplitudes and wavelengths of these waves are not uniform and not known. However, for $|G|_{\max} = 1.002014$, the amplitude can grow by a factor of 3.06×10^{10} in 12,000 steps. If the initial amplitude of the machine level error is taken to be of $O(10^{-16})$, it is reasonable to expect the amplitude of the dominant short wave to be on the order of 3×10^{-6} after 12,000 time steps, which is consistent with the order of magnitude of the short wave amplitude shown in Fig. 17. It is also noted from Fig. 16 that the amplification factor near $k = k_{\max}$ is only slightly smaller than $|G|_{\max}$ so that the wave components near $k = k_{\max}$ are also growing rapidly, but at a rate that is slightly lower than $|G|_{\max}$. After 12,000 time steps ($t = 2.4$ s), $\hat{u}_l(x)$ is characterized by the linear superposition of a packet of short waves near $k = k_{\max}$ together with the primary component ($k = k_0$), as shown in Fig. 17. Thus the observed wave amplitude can be larger than the estimate based on $|G|_{\max}$.

A similar comparison between the predicted and computed growth of the disturbance using the SOU scheme is presented next. The flow and computational parameters are: $u_l = 1$ m/s, $\Delta U = 16$ m/s, $\beta = 0$, $a_l = 0.5$, $CFL_l = 0.05$, and $N = 200$. The initial conditions for the primary disturbance are: $k_0 = 2\pi\ \mathrm{m}^{-1}$, $\varepsilon = 6.366 \times 10^{-6}$, $\varepsilon_l = 9.165 \times 10^{-7}$ m/s, and $\varepsilon_g = 2.028 \times 10^{-4}$ m/s. The maximum of $|G|$ occurs at $\phi_{\max} = 0.911062$ with $|G|_{\max} = 1.00886$. Hence the flow is analytically stable but computationally unstable. The liquid velocity disturbance after 3000 computational steps is shown in

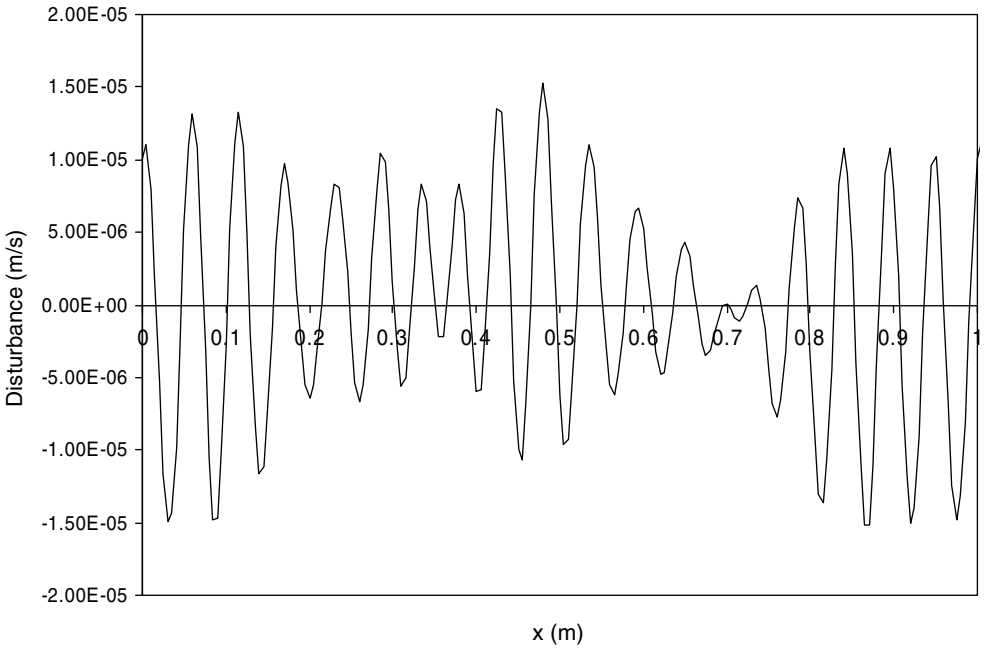

Fig. 17. Liquid velocity disturbance after 12,000 steps with FOU scheme for $N = 200$, $u_l = 0.5$ m/s, $\Delta U = 16$ m/s (well-posed), $CFL_l = 0.02$, and $\alpha_l = 0.5$.

Fig. 18. The peak-to-peak count of the short waves is $n = 29$ which matches $n_{\max} = N\phi_{\max}/(2\pi) \approx 29$ based on von Neumann stability analysis. Similar to the FOU case, the initial amplitude of the machine roundoff error is estimated to be of $O(10^{-16})$, and after 3000 steps, the short wave amplitude should reach the order of $10^{-16} \times |G|^{3000}_{\max} \approx 3 \times 10^{-5}$. This rough estimate based on $k = k_{\max}$ compares reasonably with the actual disturbance shown in Fig. 18, which consists of a packet of waves near $k = k_{\max}$.

5.4. Discussion on the growth of short waves

In the previous section, based on the peak-to-peak count and the order of magnitude estimate for the growth of the short wave amplitude, it is deduced that when the numerical scheme is unstable a packet of short waves of wavenumber near $k = k_{\max}$ originate from machine roundoff error during the computation and eventually become comparable or larger than the primary disturbance of $k_0 = 2\pi$ m^{-1}. Since the exact solution for the growth of the primary disturbance is known from the IKH analysis, it can be used to compute the solution errors from various numerical schemes. The contributions from the short waves are "unexpected" and they will contribute to the error. Since this error will grow with time from the level of machine error and eventually destroy the accuracy of the numerical solution (in capturing the growth of the primary disturbance), it is clear that the "error" assessment depends on: (i) the magnitude of the initial amplitude of the primary disturbance and (ii) the instant of time the error is computed.

To gain further insight into how the short waves interact with the targeted primary disturbance in affecting the overall accuracy assessment of the standard two-fluid model, a series of computa-

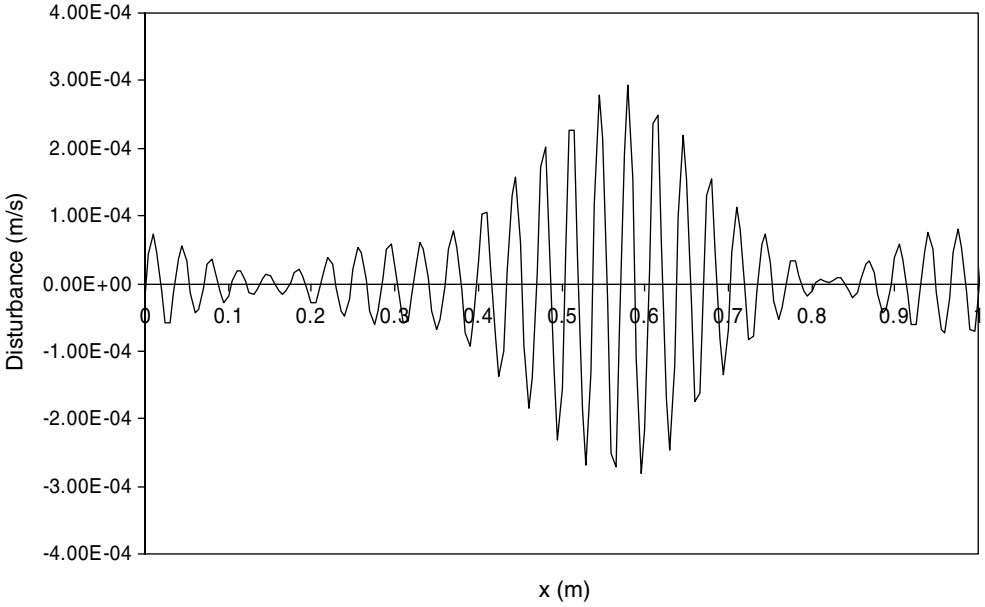

Fig. 18. Liquid velocity disturbance $\hat{u}_l$ using SOU scheme after 3000 steps of computation for $N = 200$, $u_l = 1$ m/s, $\Delta U = 16$ m/s (well-posed), $CFL_l = 0.05$, and $\alpha_l = 0.5$.

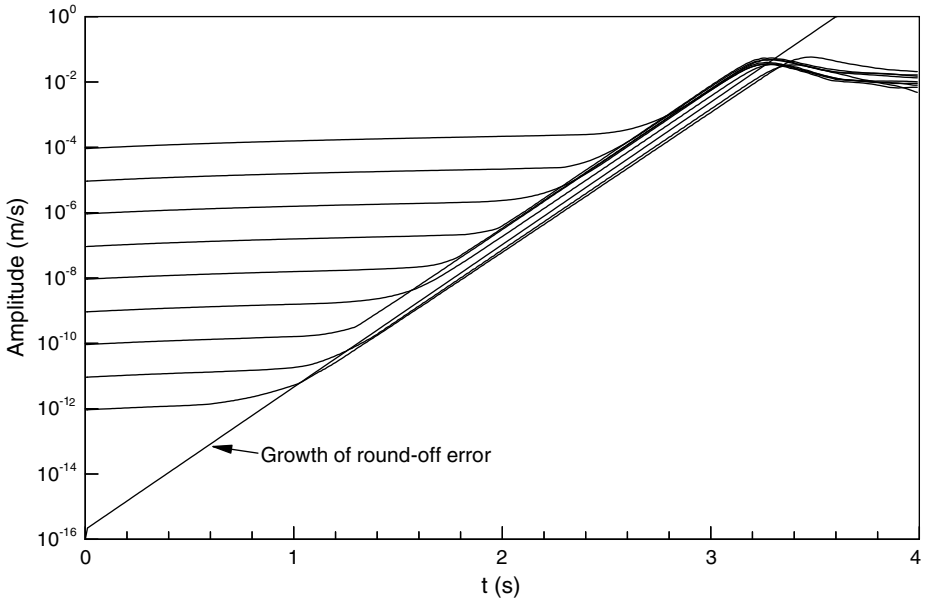

Fig. 19. Amplitude growth history of $\hat{u}_l$ for different initial amplitudes using FOU scheme.

tions is carried out using a series of initial amplitudes (ε_l ranging from 10^{-12} m/s to 10^{-4} m/s) for the liquid velocity disturbance $\hat{u}_l$. To limit the scope, only the results from the use of the FOU scheme are presented. The flow and computational parameters are the same as used in Figs. 16 and 17 except for ε_l. The maximum value of $|\hat{u}_l(x)|$ in the domain at each time step is obtained and recorded. Fig. 19 shows the variations of this maximum value as a function of time for different values of ε_l.

It is observed that during the initial stage, all amplitudes grow according to the amplification factor $|G|$ ($k_0 = 2\pi\ \mathrm{m}^{-1}$) in the form of $\varepsilon_l|G|^p$, in which ε_l is the initial amplitude of the disturbance, based on von Neumann analysis, and p denotes the pth time step. The short wave grows out of machine roundoff error independently in the form of $\varepsilon_r|G|^p_{\max}$, in which $\varepsilon_r \sim O(10^{-16})$ is the amplitude of the roundoff error whose exact value is uncertain, and $|G|_{\max} = 1.002014$ is the maximum amplification factor for the FOU scheme obtained from the von Neumann analysis. It corresponds to $\phi_{\max} = 0.596902$. Clearly, smaller values of ε_l require less time (or smaller p) for the roundoff error to catch up with the primary disturbance ($k_0 = 2\pi\ \mathrm{m}^{-1}$). The envelope of these computed amplitudes seem to roughly agree with $\varepsilon_r|G|^p_{\max}$ denoted by the thick line in Fig. 19, with ε_r taken to be 2×10^{-16}.

To understand the emergence of the packet of short waves, the disturbance $\hat{u}_l(x)$ is decomposed using discrete Fourier transform

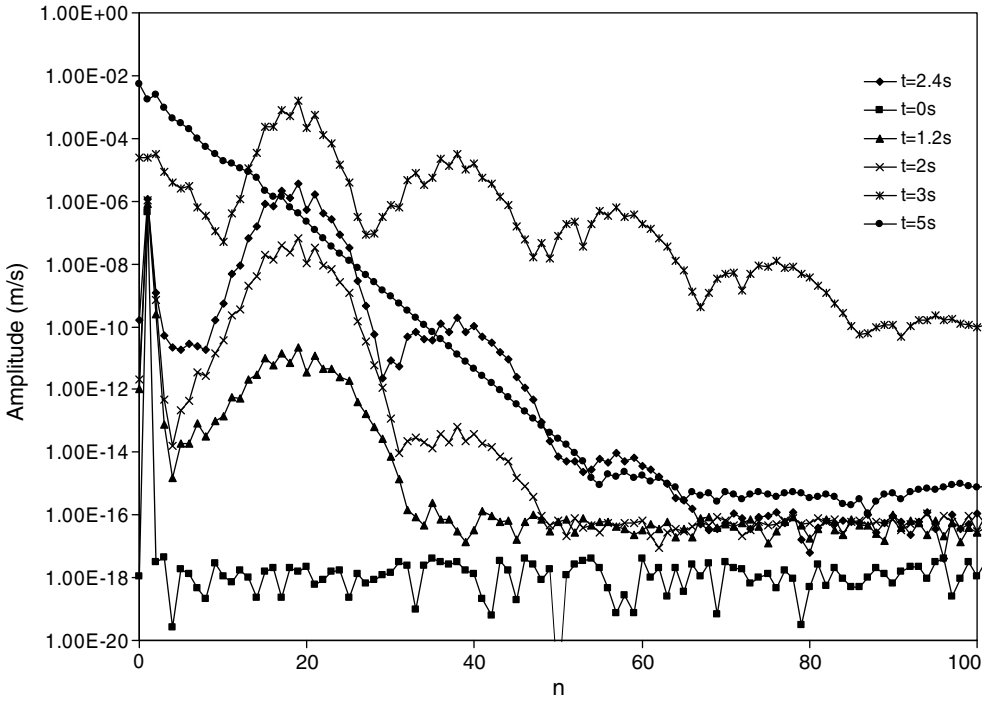

Fig. 20. Fourier components of $\hat{u}_l$ at various times using FOU scheme.

(Press et al., 1992). Fig. 20 shows the magnitude of each Fourier component for $\hat{u}_l(x)$ computed using the FOU scheme for the same conditions with which Figs. 16 and 17 are obtained as a function of $n = k/2\pi$. Since the boundary condition is periodic, n is an integer. At time $t = 0$, all wave components have the amplitude of machine roundoff error, except for the primary wave ($k_0 = 2\pi\ \mathrm{m}^{-1}$ or $n = 1$). At $t = 1.2$ s, a group of wave components near $n = 19$ have grown from the machine level noise to about 10^{-11} for their magnitudes of the Fourier coefficients. It is clear in the spectral domain that instead of just one particular wave component ($k = k_{\max}$) that is growing rapidly with time, there are about 10 other wave components near $k = k_{\max}$ which have grown to a slightly lower but similar magnitude. However this is still sufficiently below the magnitude of the primary disturbance. At $t = 2$ s, the magnitudes of this group of short waves reach about 10^{-7} while the Fourier magnitude of the primary disturbance is about 1.0768×10^{-6}. At $t = 2.4$ s, a group of higher harmonic waves emerges. The magnitude of this group peaks around $n = 38$, clearly as a result of non-linearity due to convection. At $t = 3$ s, even higher harmonics, which peak around $n = 57$, 76, and 95, also emerge. The amplitudes of these short waves (near $n = 19$, 38, and 57) have exceeded that of the primary disturbance. At $t = 5$ s, no visible peaks are observed in the spectrum and the base flow u_l and u_g are significantly different from the initially imposed state due to non-linearity and high level of numerical damping associated with the FOU scheme. This fundamental shift can also be seen in Fig. 19 as the maximum disturbance in $\hat{u}_l(x)$ starts to decrease slightly and the computation remains stable. It is also possible that the non-linearity of the discretized system becomes so strong that the numerical solution may have evolved to a different stable state. The result of von Neumann analysis is no longer applicable. This is drastically different from the case when the CD scheme is used as shown in Fig. 15. The lack of sufficient numerical damping in the CD scheme eventually causes the computation to blow up.

However, it is very clear that the "stable" result obtained using the FOU scheme at $t = 5$ s has been completely contaminated by the short wave errors and by the numerical diffusion. Such computational results are unphysical and cannot be useful for flow predictions.

5.5. Faster growth of short waves by grid refinement under ill-posed condition

Issa and Kempf (2003) demonstrated, based on the standard two-fluid model finite difference computation, that when the system is ill posed, the growth rate of the disturbance increases linearly without bound with the number of grids (N) (see their Fig. 5). Prosperetti (2007) attributed this phenomenon to the loss of hyperbolicity, and correctly pointed out that "a finer grid permits the appearance of shorter wavelengths".

Since computational analysis always deals with a discretized system, which contains a certain degree of numerical dissipation and dispersion, there is a departure from the original differential equations. An alternative but more direct and quantitative explanation for the computational phenomenon observed by Issa and Kempf (2003) can be provided by examining the growth factor $G(\phi = k\Delta x)$. Under the same flow condition and keeping the CFL numbers the same for consistency, Eqs. (34) and (35)a–c show that G is uniquely determined by $\phi = k\Delta x$. When the computation is unstable, the maximum growth occurs at $\phi = \phi_{\max}$ or equivalently at the wavenumber $k_{\max} = \phi_{\max}/\Delta x = N\phi_{\max}/L$ in which N is the number of grids and L is the length of the computational domain. Clearly, the wavelength of the most rapidly growing wave directly scales with Δx. Grid refinement with increasing N directly causes an increase in $k_{\max}$. This completely supports Prosperetti's insight that "a finer grid permits the appearance of shorter wavelengths" characterized by larger $k_{\max}$. Furthermore, as discussed in Section 5.4, the growth of the short wave of $k = k_{\max} \propto 1/\Delta x$ as a function of t can be characterized by $\varepsilon_r |G|_{\max}^{t/\Delta t}$. The value of $|G_{\max}|$ is independent of N as $\phi_{\max}$ is fixed and the exponent can be expressed as $t/\Delta t = t\frac{N\cdot u_l}{L\cdot CFL_l}$. Hence the growth rate of the short wave error is $\frac{N\cdot u_l}{L\cdot CFL_l}\log|G|_{\max}$, which is directly proportional to N. This is in complete agreement with Fig. 5 of Issa and Kempf (2003) in which the growth rate is shown to be linearly increasing with N.

Hwang (2003) analyzed the performance of various upwind schemes for hyperbolic as well as non-hyperbolic systems. For non-hyperbolic, ill-posed problems, an accurate solution was obtained before the short waves eventually contaminate the solution. In particular, Fig. 4 of Hwang (2003) showed that for an ill-posed condition, the successive grid refinement initially yields a decrease in error and then an increase in the error at a fixed time.

To directly illustrate the effect of the grid refinement on the solution and on the growth of the short wave error, computations are performed on three sets of grids ($N = 100$, 200, and 400) using the FOU scheme under the same conditions as used to generate Figs. 16 and 17; the numerical scheme is unstable under such conditions. The CFL numbers are kept the same in all three sets of grids. Fig. 21 shows the maximum value of $|\hat{u}_l(x)|$ as a function of the time step. After about 10,000 time steps, the short waves take over and completely contaminate the growth of the primary disturbance. Moreover, the growth of the short waves follows nearly the same curve which can be described by $\varepsilon_r |G|_{\max}^{t/\Delta t}$ where $|G|_{\max}$ is the same for all N's since $\phi_{\max} = k_{\max}\Delta x = 0.596902$ is the same under the same flow conditions and same CFL numbers. Thus, when plotted against time, the growth of the short waves on a finer grid (thus smaller Δt) computation will be much faster.

In Fig. 4 of Hwang's (2003) paper, it was shown that the solution error reaches a minimum as the grid is refined; further refinement of the grids results in a rapid increase in the error. This is true for both the FOU scheme and the Fromm scheme. Prosperetti (2007) attributed such a minimum of solution error as function of Δx to the rapid growth of the short wave "as soon as the unstable modes become possible".

Fig. 22 illustrates the effect of grid density on the solution accuracy with the FOU and CD schemes for the same flow conditions used for Fig. 17. At $t = 2.4$, the computational result from various grids are obtained and compared with the exact result of IKH analysis. It is noted that the flow is in a well-posed condition so that the amplitude of the analytical solution for the primary disturbance remains constant.

For larger Δx, the computational error of the primary disturbance decreases as Δx is reduced because the truncation error decreases with smaller Δx. The error of the CD scheme decreases faster than that of FOU because of the 2nd-order accuracy. The further decrease in Δx leads to dramatically larger error for the FOU scheme. This is because $\varepsilon_r |G|_{\max}^{t/\Delta t}$ increases rapidly as Δt decreases for the fixed $t = 2.4$. For this flow and computational condition, however, the CD scheme is stable and short waves do not grow out of the roundoff error. Hence the truncation error continues to decrease as Δx decreases. The CD scheme is clearly superior to the FOU scheme.

Fig. 23 shows the effect of grid density on the solution accuracy with the FOU and CD schemes at the ill-posed condition. Both FOU and CD schemes are unstable under this condition. The solution error using each scheme first decreases as Δx is reduced because of the decrease in the truncation error, and the growing roundoff error has not reached comparable magnitude. The solution error reaches a minimum and then the growing roundoff error becomes comparable with the truncation error. Finally the solution error increases rapidly with smaller Δx. The slope of the error curve in the log–log plot for larger values of Δx is 1 for the FOU and 2 for the CD schemes due to the difference in the order of the truncation errors.

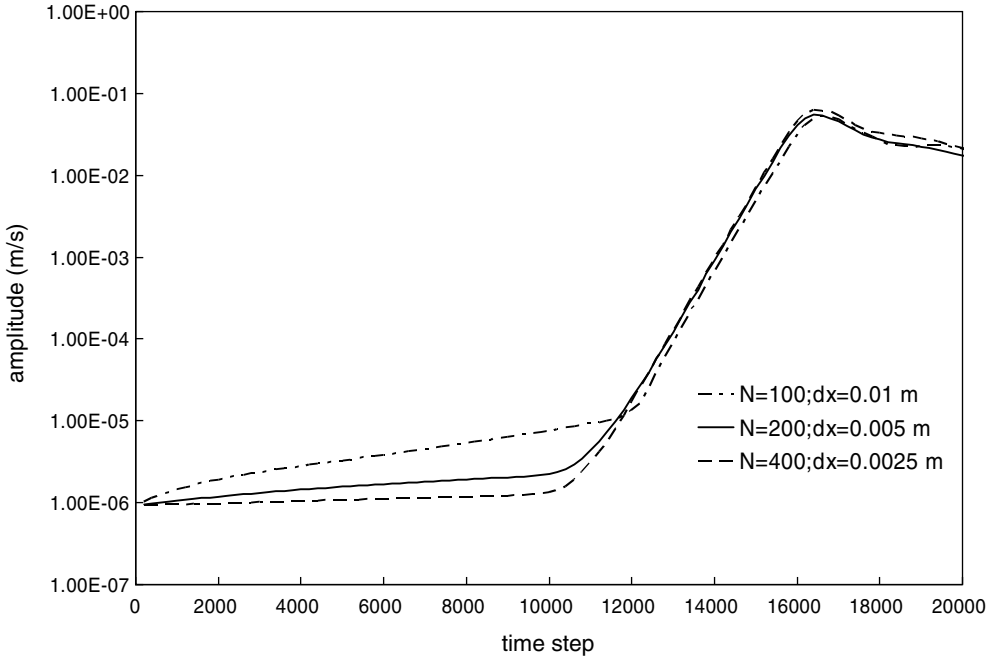

Fig. 21. Amplitude growth history of $\hat{u}_l$ as a function of time step with various grid sizes using FOU scheme.

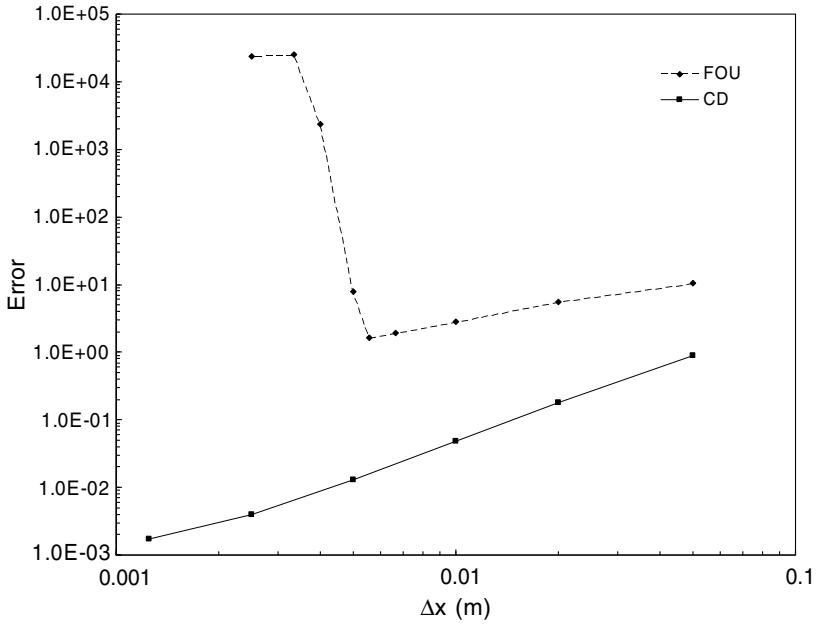

Fig. 22. Solution error of FOU and CD schemes as a function of grid size at $t = 2.4$ s. The system is well-posed for $u_l = 0.5$ m/s, $\Delta U = 16$ m/s, $CFL_l = 0.02$, and $\alpha_l = 0.5$.

Although the solution for the growing primary disturbance itself is no longer physically relevant, Fig. 23 shows that the CD scheme can more accurately predict the growth of the disturbance than the FOU scheme for small time.

In either case shown in Figs. 22 and 23, once the scheme becomes computationally unstable ($|G|_{\max} > 1$) for an otherwise well posed problem (Fig. 22) or when the physical problem becomes ill-posed (Fig. 23), it is only prudent to refrain from fine tuning the computation by finding a grid that gives minimum error. A sound computational practice is to perform the standard grid refinement test to ensure the consistency of the numerical scheme before the true machine roundoff error is reached. Attempts to identify an optimum grid, that yields a balance between a well behaved truncation error and a fully blown (or rapidly growing) short wave error due to ill-posedness or an unstable algorithm, are not useful since the numerical solutions to such a two-phase flow problem carry little physical meaning. The results shown in Fig. 23 are not an endorsement for pursuing an "accurate" solution for an ill-posed problem. Rather, they merely demonstrate that the CD scheme is more accurate for standard two-fluid model than the FOU scheme.

5.6. Wave growth in the standard viscous two-fluid model

The foregoing discussions have demonstrated that the CD scheme has the best stability characteristics for the standard inviscid two-fluid model comparing with FOU, SOU, and QIUICK

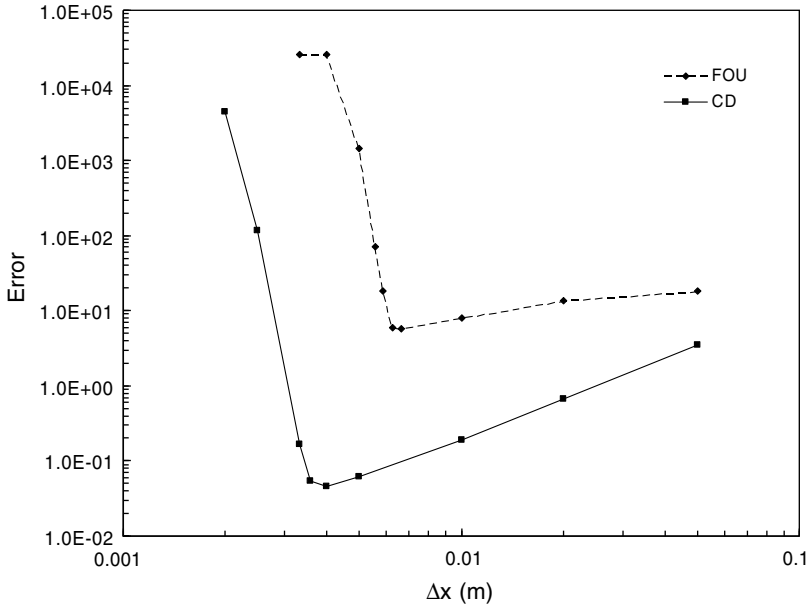

Fig. 23. Solution error of FOU and CD schemes as a function of grid density at $t = 2.4$ s. The system is ill-posed for $u_l = 0.5$ m/s, $\Delta U = 16.5$ m/s, $CFL_l = 0.02$, and $\alpha_l = 0.5$.

schemes. A similar comparison is conducted for the standard viscous two-fluid model and the results are presented in this section. The main focus is on the flow condition when the viscous Kelvin–Helmholtz instability has occurred while the inviscid Kelvin–Helmholtz instability has not occurred. In other words, the system remains well-posed although a small disturbance introduced on the system can grow until: (i) excessive numerical damping and the non-linearity restabilizes the computation; or (ii) the computation blows up due to the interface reaching the top wall implying that the stratified flow transits to slug flow. The present work does not emphasize on developing numerical strategies to force the transition; and the termination of the computation in the event the liquid volume fraction becomes one is interpreted as the transition point from the stratified flow to slug flow.

Before examining the amplification factor, it is important to note that when the problem is well-posed but VKH unstable, it is necessary for the magnitude of the amplification factor, $|G|$, to exceed one for some wavelengths which allows the true solution for the fluid velocities to grow with time. The computational stability condition thus should be extended to (Hwang, 2003):

$$|G_{num}|_{max} < \max\{1, |G_{exact}|_{max}\}.$$

For illustration purposes, water and air are used as examples, and the pipe diameter is 0.05 m. The computational domain is 1 m long, the grid number is $N = 200$. The pipe inclination angle is set to $\beta = 0$ for the stability analysis; but it is set to a negative value in the finite difference computation in order for the gravitational force to overcome the interfacial drag while maintaining the periodic boundary condition. Fig. 24 compares the amplification factor $|G|$ of four different discretization schemes and the analytical amplification factor using VKH instability analysis. The liquid velocity is $u_l = 0.6881$ m/s, the gas velocity is $u_g = 10.64$ m/s, void fraction

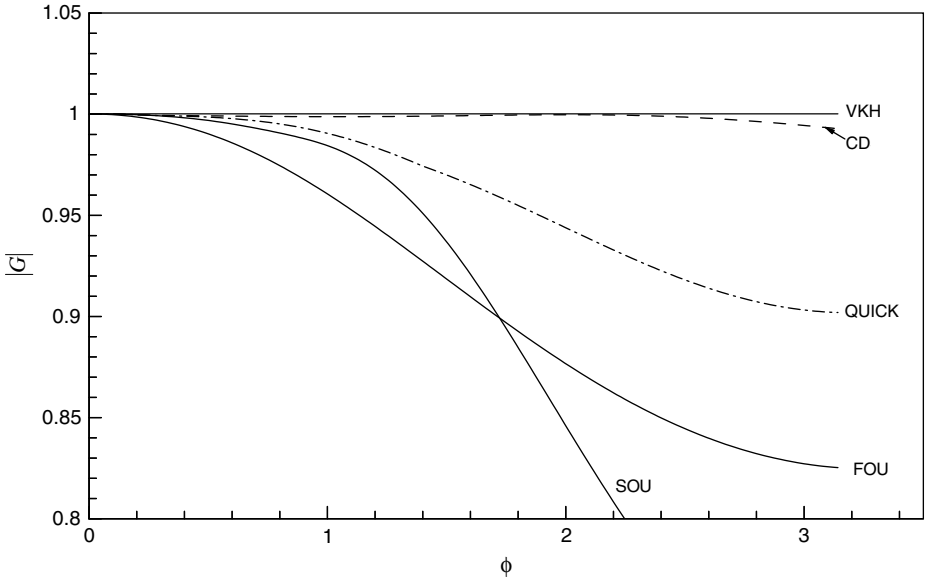

Fig. 24. Amplification factors of different schemes using standard viscous two fluid model for $N = 200$, $\alpha = 0.4360$, $u_l = 0.6881$ m/s, $u_g = 10.64$ m/s, and $CFL_l = 0.1$.

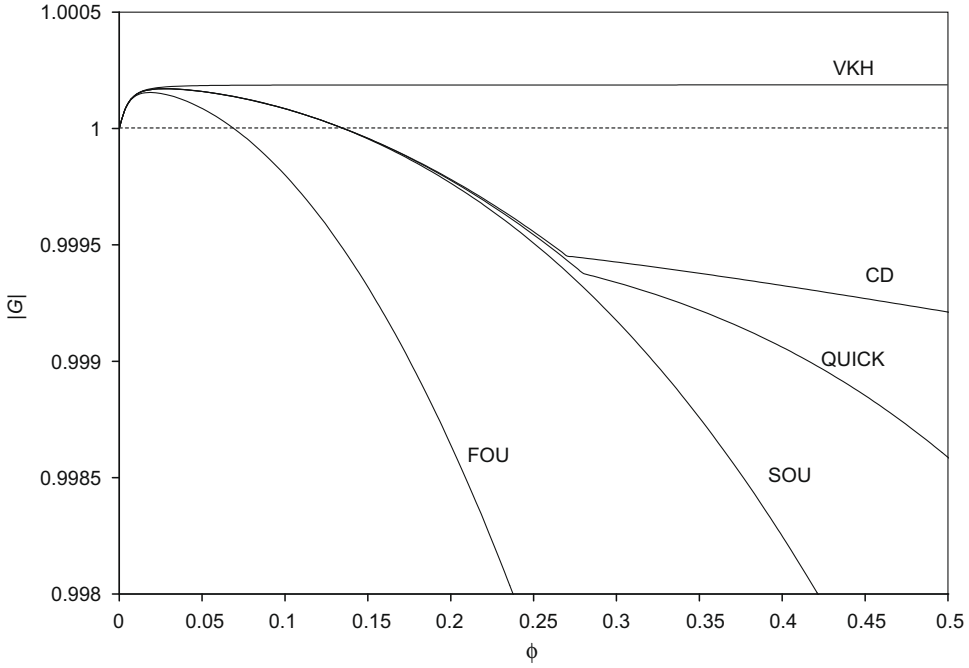

Fig. 25. Amplification factors of different schemes at low k using standard viscous two fluid model for $N = 200$, $\alpha = 0.4360$, $u_l = 0.6881$ m/s, $u_g = 10.64$ m/s, and $CFL_l = 0.1$.

is $\alpha = 0.4360$, and $CFL_l = 0.1$. Thus, the system of equations is well-posed but the slip velocity slightly exceeds the one needed for developing the VKH instability based on the theoretical analyses. The VKH amplification factor curve is flat after a certain wavenumber and slightly higher than one. The amplification factor of the CD scheme is slightly lower than one but quite close to one, except at the low k, where $|G| > 1$. The FOU scheme possesses excessive numerical damping at high k. The SOU scheme possesses larger numerical damping than that for the FOU scheme at high k. The performance of the QUICK scheme is between those of CD and the FOU schemes. The results shown in Fig. 24 generally agree with those of the standard inviscid two-fluid model. However, shear stresses cause the flow instability to occur at lower k for the viscous two-phase flow.

Fig. 25 shows an enlarged view of Fig. 24 near $\phi = k\Delta x = 0$. At an extreme low k range, the amplification factors of all schemes agree well with prediction of the VKH analysis, but when k is slightly larger, the $|G(\phi)|$ quickly deviates from that of the exact VKH analysis. For the growth of the disturbance of certain wavenumber k to be accurately captured, the grid size Δx has to be extremely small. It is also seen in Fig. 25 that $|G(\phi)|$ of FOU scheme is far from those of the CD, SOU, and QUICK schemes. This reflects the fact that FOU is only 1st-order accurate while the other three schemes all have 2nd-order accuracy.

To validate the pressure correction scheme for the standard viscous two-fluid model, comparisons between the computed wave growth and the analytical wave growth predicted using the von Neumann stability analysis are presented. Fig. 26 shows the

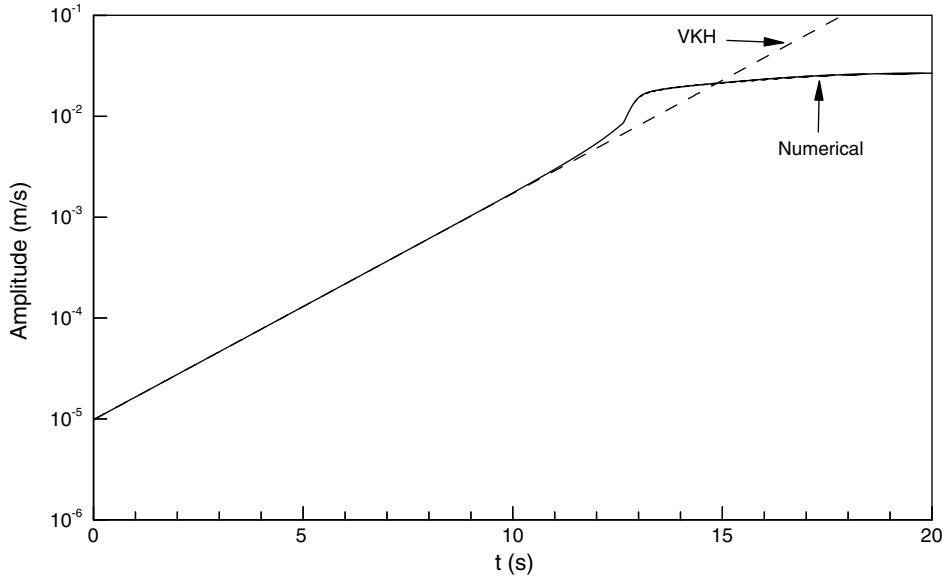

Fig. 26. Amplitude growth history of $\hat{u}_l$ using CD scheme for $N = 200$, $u_l = 2$ m/s, $u_g = 0.998174$ m/s, $\beta = -0.0617144$, $\alpha_l = 0.98$, and $CFL_l = 0.05$.

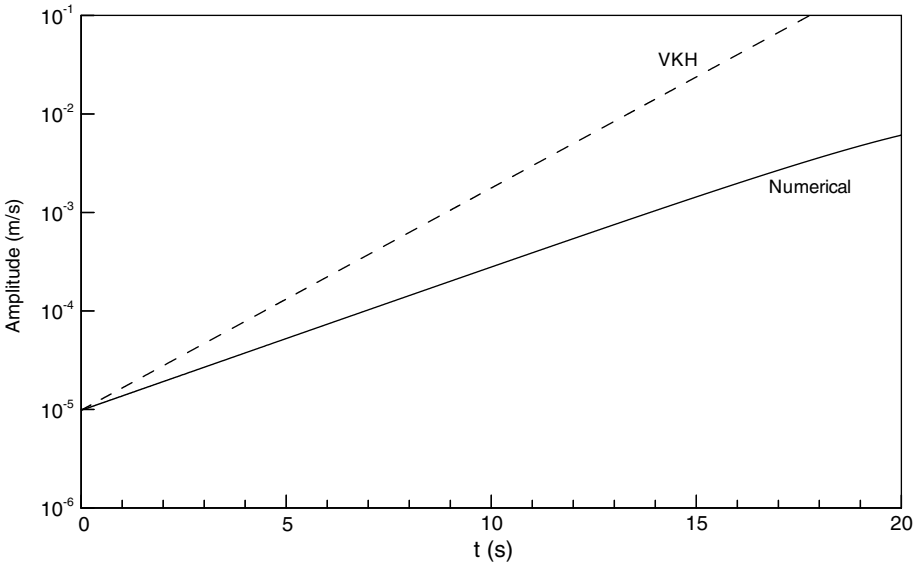

Fig. 27. Amplitude growth history of $\hat{u}_l$ using FOU scheme for $N = 200$, $u_l = 2$ m/s, $u_g = 0.998174$ m/s, $\beta = -0.0617144$, $\alpha_l = 0.98$, and $CFL_l = 0.05$.

growth history of a harmonic with $k_0 = 2\pi m^{-1}$ using the CD scheme. The parameters used are $u_l = 2$ m/s, $u_g = 0.998174$ m/s, $\beta = -0.0617144$, and $a_l = 0.98$. The system is well-posed but the flow is VKH unstable. The amplitude of the disturbance grows exponentially with time as shown in Fig. 26. The numerical solution agrees extremely well with the prediction using VKH analysis. Based on the von Neumann stability analysis for the CD scheme, it is predicted that the amplitude from $t = 0$ to $t = 10$ s increases by a factor of 174.75. The computed amplitude ratio is 176.86 with a difference of 1.21% for a period of 10 s. Furthermore, the amplification factor $|G|$ for each time step using the VKH analysis is 1.00006491 and the von Neumann analysis gives $|G(k_0\Delta x)| = 1.00006454$. This excellent agreement is not surprising since the CD scheme has been demonstrated to have excellent numerical accuracy when it is applied to the standard inviscid two-fluid model. During the final stage of growth, the amplitude of the wave is no longer small, so the small amplitude assumptions used for the von Neumann stability analysis and the VKH instability analysis are invalid. Thus, the waves enter a non-linear growth stage and the numerical amplification factor no longer matches the analytical prediction.

Using the same computational parameters, the growth history of the disturbance for the FOU scheme is shown in Fig. 27. It is noted that $|G(k_0\Delta x)| = 1.00004197$ for the FOU scheme, which is much smaller than 1.00006491 from the VKH analysis. The smaller value in $|G|$ is the result of numerical damping inherent with the FOU scheme. Fig. 27 highlights the discrepancy in the amplitude growth between the VKH prediction and the FOU scheme.

The foregoing assessment shows that the pressure correction scheme can be quite accurate in predicting the growth of a wave or disturbance for both standard inviscid and viscous two-fluid models. It also clearly shows that the 1st-order upwind scheme possesses excessive numerical damping while the central difference scheme has a much better numerical accuracy and is better suited for the standard viscous two-fluid model.

6. Conclusions

Numerical instability for the standard two-fluid model near the ill-posed condition is investigated for various discretization schemes with an Euler implicit method for the time derivatives, while the pressure correction method is used to obtain the pressure. The von Neumann stability analysis is carried out to obtain the amplification factor of a small disturbance in the discretized system. The central difference scheme has the best stability characteristics in handling the standard two-fluid model, followed by the QUICK scheme. The excessive numerical diffusion in the 1st-order upwind scheme does not lead to an improvement in the numerical stability; instead, it seems to promote numerical instability in comparison with the central difference scheme and result in a smaller critical slip velocity beyond which the disturbance grows. Despite its nominal 2nd-order accuracy and popularity, the 2nd-order upwind scheme is much more unstable than the 1st-order upwind scheme when it is applied to solve the standard two-fluid model equations.

For an initially specified primary long wavelength disturbance, the amplitude will decay according to the amplification factor for the given wavenumber and grid size due to numerical dissipation if the scheme is stable. When the computation becomes unstable either because of ill-posedness or because of a poor choice of computational strategy or parameters, the computed disturbance will first grow according to the amplification factor for the long wave and then it will grow at a much higher rate for a packet of short waves which correspond to the highest amplification factor. Due to the quadratic non-linearity of the convection terms in the system, frequency doubling is observed and shorter waves emerge from the computation. With the excessive numerical dissipation and the distortion caused by non-linearity, it is possible for the computation to continue and restabilize. However when there is a very low numerical dissipation, non-linear effects are not enough to prevent the computation from blowing up. Thus, such computational results for an ill-posed problem or unstable computational condition are not reliable and should not be pursued.

The results of the present study on the standard inviscid two-fluid model suggest that the computational instability is largely the property of the discretized standard two-fluid model but it is also strongly affected by the inherent ill-posedness of the standard two-fluid model differential equations when the slip velocity is close to the critical value for the system to become ill-posed.

For the standard viscous two-fluid model, the central difference scheme is also found to be superior to the upwind and QUICK schemes in terms of the computational accuracy when the Euler implicit method is used for the time derivatives. The pressure correction method works well for both standard inviscid and viscous two-fluid models as long as the system is well-posed.

Acknowledgements

This work was supported by NASA Glenn Research Center under contract NAG3-2930 and NASA Kennedy Space Center. The authors are very grateful to Professor Andrea Prosperetti for the many useful comments and suggestions he provided during the revision stage of this work.

References

Ansari, M.R., Shokri, V., 2007. New algorithm for the numerical simulation of two-phase stratified gas-liquid flow and its application for analyzing the Kelvin – Helmholtz instability criterion with respect to wavelength effect. Nucl. Eng. Des. 237, 2302–2310.

Barnea, D., Taitel, Y., 1994. Interfacial and structural stability of separated flow. Int. J. Multiphas. Flow 20, 387–414.

Brauner, N., Maron, D.M., 1992. Stability analysis of stratified liquid–liquid flow. Int. J. Multiphas. Flow 18, 103–121.

Chan, A.M.C., Banerjee, S., 1981. Refilling and rewetting of a hot horizontal tube part II: structure of a two-fluid model. J. Heat Transf. 103, 287–292.

Ferziger, J.H., Peric, M., 1996. Computational Methods for Fluid Dynamics. Springer, Berlin.

Gidaspow, D., 1974. Modeling of two phase flow. Proceedings of the 5th International Heat Transfer Conference VII.

Hirsch, C., 1988. Numerical Computation of Internal and External Flows, vol. I: Fundamentals of Numerical Discretization. John Wiley & Sons, New York.

Hwang, Y-H., 2003. Upwind scheme for non-hyperbolic systems. J. Comput. Phys. 192, 643–676.

Ishii, M., 1975. Thermo-Fluid Dynamic Theory of Two Phase Flow. Eyrolles, Paris.

Issa, R.I., Kempf, M.H.W., 2003. Simulation of slug flow in horizontal and nearly horizontal pipes with the two-fluid model. Int. J. Multiphas. Flow 29, 69–95.

Issa, R.I., Woodburn, P.J., 1998. Numerical prediction of instabilities and slug formation in horizontal two-phase flows. 3rd International Conference on Multiphase Flow. Lyon, France.

Jones, A.V., Prosperetti, A., 1985. On the stability of first-order differential models for two-phase flow prediction. Int. J. Multiphas. Flow 11, 133–148.

Liao, J., 2005. Modeling two-phase transport during cryogenic chilldown in a pipeline, Ph.D. dissertation. University of Florida.

Liles, D.R., Reed, W.H., 1978. A semi-implicit method for two-phase fluid dynamics. J. Comput. Phys. 26, 390–407.

Lin, P.Y., Hanratty, T.J., 1986. Prediction of the initiations of slugs with linear stability theory. Int. J. Multiphas. Flow 12, 79–98.

Lin, P.Y., Hanratty, T.J., 1987. Detection of slug flow from pressure measurement. Int. J. Multiphas. Flow 13, 13–21.

Lyczkowski, R.W., Gidaspow, D., Solbrig, C.W., Hughes, E.D., 1978. Characteristics and stability analyses of transient one-dimensional two-phase flow equations and their finite difference approximations. Nucl. Sci. Eng. 66, 378–396.

Mahaffy, J.H., 1982. A stability enhancing two-step method for fluid flow calculations. J. Comput. Phys. 46, 329–341.

Ohkawa, T., Tomiyama, A., 1995. Applicability of high-order upwind difference methods to the two-fluid model. Advances in Multiphase Flow. Elsevier Science. pp. 227–240.

Patankar, S.V., 1980. Numerical Heat Transfer and Fluid Flow. McGraw-Hill, New York.

Press, W.H., Flanery, B.P., Teukolsky, S.A., Vetterling, W.T., 1992. Numerical Recipes in FORTRAN. Cambridge University Press, Cambridge, UK.

Prosperetti, A., 2007. Average equations. In: Prosperetti, A., Tryggvason, G. (Eds.), Computational Methods for Multiphase Flow. Cambridge University Press, Cambridge, UK.

Ramshaw, J.D., Trapp, J.A., 1978. Characteristics, stability, and short-wavelength phenomena in two-phase flow equation systems. Nucl. Sci. Eng. 66, 93–102.

Shieh, A.S.-L., 1994. Stability, accuracy and convergence of the numerical methods in RELAP5/MOD3. Nucl. Sci. Eng. 116, 227–244.

Song, J.H., Ishii, M., 2000. The well-posedness of incompressible one-dimensional two-fluid model. Int. J. Heat Mass Transf. 43, 2221–2231.

Stewart, B.H., 1979. Stability of two-phase flow calculation using two-fluid models. J. Comput. Phys. 33, 259–270.

Taitel, Y., Dukler, A.E., 1976. A model for predicting flow regime transition in horizontal and near horizontal gas liquid flow. AIChE J. 22, 47–55.

Wallis, G.B., 1969. One-Dimensional Two-Phase Flow. McGraw-Hill, New York.